

Human-In-The-Loop Person Re-Identification

Hanxiao Wang, Shaogang Gong, Xiatian Zhu, and Tao Xiang

Abstract—Current person re-identification (re-id) methods assume that (1) pre-labelled training data is available for every camera pair, (2) the gallery size is moderate in model deployment. However, both assumptions are invalid in real-world applications where camera network and gallery size increase dramatically. Under such more realistic conditions, human involvement is often inevitable to verify the results generated by an automatic computer algorithm. In this work, rather than proposing another fully-automated and yet unrealistic re-id model, we introduce a semi-automatic re-id solution. Our goal is to minimise human efforts spent in re-id deployments, while maximally drive up re-id performance. Specifically, a *hybrid* human-computer re-id model based on Human Verification Incremental Learning (HVIL) is formulated which does not require any pre-labelled training data, therefore scalable to new camera pairs; Moreover, this HVIL model learns cumulatively from human feedback to provide an instant improvement to re-id ranking of each probe on-the-fly, thus scalable to large gallery sizes. We further formulate a Regularised Metric Ensemble Learning (RMEL) model to combine a series of incrementally learned HVIL models into a single ensemble model to be used when human feedback becomes unavailable. We conduct extensive comparative evaluations on three benchmark datasets (CUHK03, Market-1501, and VIPeR) to demonstrate the advantages of the proposed HVIL re-id model over state-of-the-art conventional human-out-of-the-loop re-id methods and contemporary human-in-the-loop competitors.

Index Terms—Person re-identification, human-in-the-loop, human-out-of-the-loop, interactive model learning, human-machine interaction, human labelling effort, human verification, hard negative mining, incremental model learning, metric ensemble.



INTRODUCTION

PERSON re-identification (re-id) is the problem of matching people across non-overlapping camera views distributed in open spaces at different locations, typically achieved by matching detected bounding box images of people [23]. This is an inherently challenging problem due to the potentially dramatic visual appearance changes caused by uncontrolled variations in human pose and unknown viewing conditions on illumination, occlusion, and background clutter (Fig. 1). A re-id model is required to differentiate images of different categories (persons) with similar appearances, which can be considered as solving a fine-grained visual categorisation problem [14,78], whilst also able to recognise a same category (person) with visually dissimilar appearances. Unlike conventional biometrics identification problems, e.g. face recognition, a person re-id model has *no labelled training data on target classes*, i.e. similar to a *zero-shot learning* problem [31] that requires the model to perform inherently transfer learning between a training population (seen) and a target population (unseen). Moreover, person re-id requires implicitly a model to perform *cross-domain transfer learning* [53] if each camera view is considered as a specific domain of potentially significant difference to other domains (views). This is more difficult than a standard zero-shot learning problem.

Current re-id methods are dominated by supervised learning techniques [23,34,38,39,40,50,55,79,80,88,94,97], which typically employ a “*train-once-and-deploy*” scheme (Fig. 2(a)). That is, a pre-labelled training dataset of pairwise true- and false-matching



(a) Cross-view appearance variations (b) Similar appearance among different people

Fig. 1. Person re-identification Challenges. (a) A significant visual appearance change of the same person across camera views. (b) Strong appearance similarities among different people.

identities (training population) is collected by human annotators for every pair of cameras through manually examining a vast pool of image/video data. This training dataset is used to train an offline re-id model. It is tacitly assumed by most that such a trained model can be deployed plausibly as a *fully automated* solution to re-identify target (unseen during model training) person images at test time, without any human assistance nor model adaptation. Based on this assumption, the re-id community has witnessed ever-increased matching accuracies on increasingly larger sized benchmarks of more training identity classes over the past two years. For instance, the CUHK03 benchmark [38] contains 13,164 images of 1,360 identities, of which 1,260 are used for training and 100 for testing, significantly larger than the earlier VIPeR [25] (1,264 images of 632 people with 316 for training) and iLIDS [96] (476 images for 119 people with 69 for training). The state-of-the-art Rank-1 accuracy on CUHK03 has exceeded 70% [86], tripling the best performance reported only two years ago [38].

Despite such rapid progresses, current automatic re-id solutions remain ill-suited for a practical deployment. This is because: **(1)** A manually pre-labelled pairwise training data set *for every camera pair* does not exist, due to either being prohibitively expensive to collect in the real-world as there are a quadratic number of camera pairs, or nonexistence of sufficiently large number of training people reappearing in every pair of camera

- Hanxiao Wang is with the Electrical and Computer Engineering Department, Boston University, US. Email: hwx@bu.edu. Shaogang Gong and Tao Xiang are with the School of Electronic Engineering and Computer Science, Queen Mary University of London, UK. Email: s.gong@qmul.ac.uk, t.xiang@qmul.ac.uk. Xiatian Zhu is with Vision Semantics Ltd., London, UK. Email: eddy@visionsemantics.com.

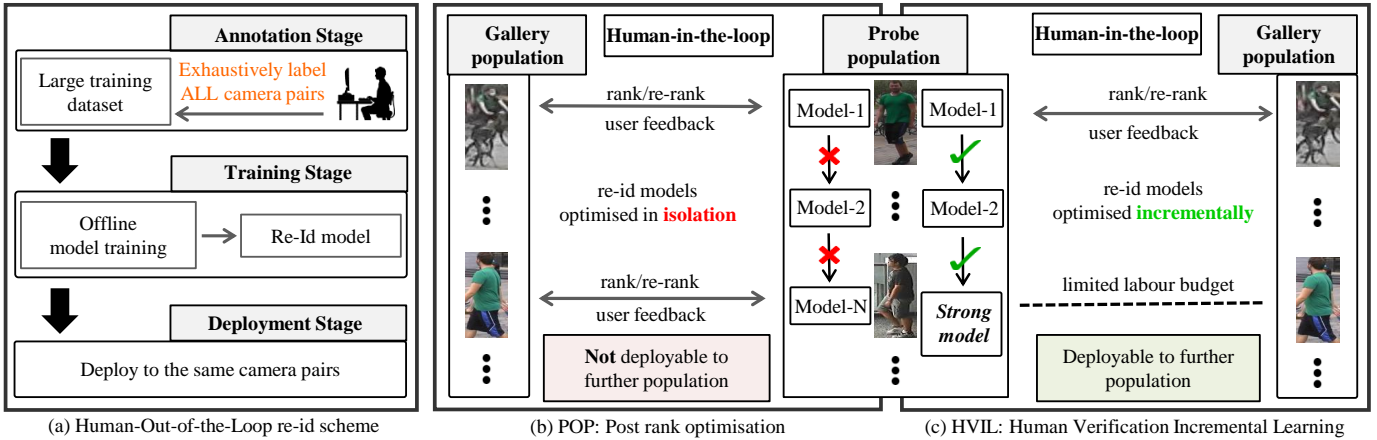


Fig. 2. Illustration of two person re-id schemes. (a) The conventional *Human-Out-of-the-Loop* (HOL) re-id scheme requires exhaustive pre-labelled training data collection for supervised offline model learning. The learned model is assumed sufficiently generalisable and then deployed to perform fully automated person re-id tasks without human in the loop. (b) POP [44]: A recent *Human-In-the-Loop* (HIL) re-id approach which optimises probe-specific models in isolation from human feedback verifications in the deployment time. All probe people requires human in the loop. (c) HVIL: The proposed new incremental HIL re-id model capable of not only progressively learning a generalised model from human verifications across all probed people while carrying out the HIL re-id tasks, but also performing the HOL re-id tasks when human effort becomes unavailable.

views. (2) Assuming the size of the training population is either significantly greater or no less than that of the target population is unrealistic. For instance, the standard CUHK03 benchmark test defines the training set having paired images of 1,260 people from six different camera views (on average 4.8 image samples per person per camera view), whilst the test set having only 100 identities each with a single image. The test population is thus 10 times smaller than the training population, with approximately 50 times less images. In practice, any deployment gallery size (test population) is almost always much greater than any labelled training data size even if such training data were available. In a public space such as an underground station, there are easily thousands of people passing through a camera view every hour [1], with a typical gallery population size of over 10,000 per day. We observed on the CUHK03 dataset that, only a 10-fold increase in gallery size leads to a 10-fold decrease in re-id Rank-1 performance, leading to a single-digit Rank-1 score, even when the state-of-the-art re-id models were trained from sufficiently sized labelled data. Given such low Rank-1 scores, in practice human operators (users) would still be required to verify any true match of a probe from an automatically generated ranking list.

In this work, we explore an alternative approach to person re-id by formulating a hybrid human-computer learning paradigm with humans in the model matching loop (Fig. 2(c)). We call this semi-automated scheme *Human-In-the-Loop* (HIL) re-id, designed to optimise re-id performance given a small number of human verification feedback and a larger-sized test population, as compared to the conventional *Human-Out-of-the-Loop* (HOL) re-id models that are mostly designed to optimise re-id given a larger-sized pre-labelled training data and a small-sized test population. This HIL re-id scheme has three significant advantages over the conventional HOL models: (1) *Less human labelling effort*: HIL re-id requires much less human labelling effort, since it does not necessarily require the expensive construction of a pre-labelled training set. More importantly, it prioritises directly the human labour effort on each given re-id task in deployment, rather than optimising the model learning error on an independent training set. More specifically, the number of feedback from human verification is typically in *tens* as compared to *thousands* of offline pre-labelled training data required by HOL methods. (2)

Model transfer learning: Our HIL model is able to achieve greater transferability with better re-id performance in test domains. This is because a HIL model focuses on re-id matching optimisation directly in the deployment gallery population, rather than learning a distance metric from a separate training set and *assuming* its blind transferability to independent (unseen) test data. It enables a human operator to interactively validate model matching results for each re-id task and inform on model mistakes (similar in spirit to hard negative mining). (3) *Reinforcing visual consistency*: As computer vision algorithms are intrinsically very different from the human visual system, a re-id model can make mistakes that generate “unexpected” (visually inconsistent) re-id ranking results, readily identifiable by a human observer. By learning directly from the inconsistency between a computer vision model and human observation, a HIL re-id model is guided to maximise visually more consistent ranking lists favoured by human observations, and thus rendering the learned model more discriminative and capable of avoiding future mistakes that seem insensible to human observation.

The main **contribution** of this work is a novel HIL re-id model that enables a user to re-identify rapidly a given probe person image after only a handful of feedback verifications even when the search gallery size is large. More specifically, a *Human Verification Incremental Learning* (HVIL) model (Fig. 2(c)) is formulated to *simultaneously* minimise human-in-the-loop feedback and maximise model re-id accuracy by incorporating: (1) *Sparse feedback* - HVIL allows for easier human feedback on a few dissimilar matching results without the need for exhaustive eyeball search of true/false in the entire rank list. It aims to rectify rapidly unexpected model mistakes by focusing *only* on minimising visually obvious errors (hard negatives) identified by human observation. This is reminiscent to learning by hard negative mining but *with* human in the loop, so to improve model learning with less training data. (2) *Immediate benefit* - HVIL introduces a new online incremental distance metric learning algorithm, which enables real-time model response to human feedback by rapidly presenting a freshly optimised ranking list for further human feedback, quickly leading to identifying a true match. (3) *The older the wiser* - HVIL is updated cumulatively on-the-fly utilising multiple user feedback per probe, with incremental

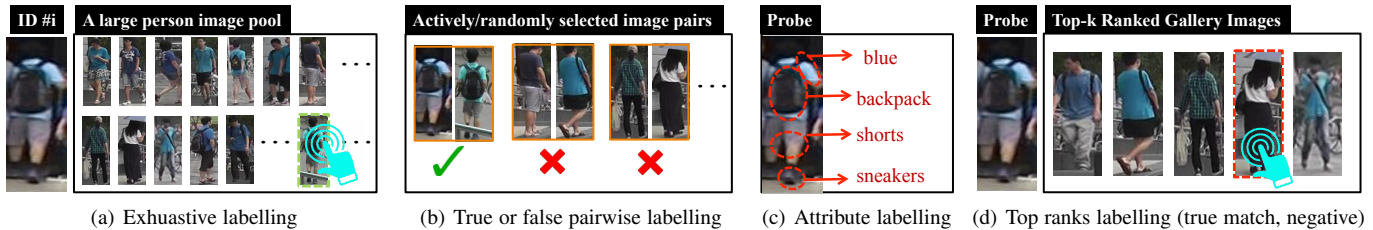


Fig. 3. Different human labelling processes are employed in person re-id model training and deployment. (a) Large size offline labelling of cross-view positive- and negative-pairs of training data with identity labels [40,52,75,91]. (b) Selective or random sampling of person image pairs for human verification in either model training [48] or deployment [15]. (c) Fine-grained attribute labelling in either training [64] or deployment [15]. (d) True match verification among the top ranked sub-list in model deployment [26,44,76], or verification of both visually dissimilar and similar wrong matches in top ranks (strong/hard and weak negative mining) in model deployment [44,76].

model optimisation for each new probe given what have been learned from all previous probes. (4) A *strong ensemble model* - An additional Regularised Metric Ensemble Learning (RMEL) model is introduced by taking all the incrementally optimised per-probe models as a set of “weak” models [4,59] and constructing a “strong” ensemble model for performing HOL re-id tasks when human feedback becomes unavailable. Extensive comparative experiments on three benchmark datasets (CUHK03 [38], Market-1501 [95], and VIPeR [25]) demonstrate that this HVIL model outperforms the state-of-the-art methods for both the proposed new HIL and the conventional HOL re-id deployments.

2 RELATED WORK

Person Re-Identification Current best performing person re-id methods are fully supervised and require a large number of pre-labelled training data (Fig. 3(a)) from every camera pair for building camera-pair specific distance metric models [18,22,34,39,40,49,50,52,55,75,79,80,88,91,94,97]. Their usability and scalability are inherently limited in real-world applications especially with large camera networks. This problem becomes more acute for the more recent data-hungry deep learning based methods [2,10,18,18,38,62,67,69,73,86,92] which need more labelled training data to function. To relax this need for intensive labelling, existing attempts include semi-supervised [33,45], unsupervised [19,32,74,93], and transfer learning [37,46,47,81]. However, all of these strategies are weak in performance compared to fully supervised learning - without labelled data, they are unable to learn strong discriminative information for cross-view re-identification. In general, all existing methods are aimed for automated HOL re-id deployment, thus suffering from dramatic performance degradation given a small size training population, even with the best state-of-the-art supervised method [39,40,49,75,88,91], as can be seen in our evaluations. In contrast, the proposed HVIL model learns interactively from human online feedback equivalent to a smaller number of *selective* labelling of negative-pair data on-the-fly, therefore costing less human “labelling effort”. This HVIL approach to re-id yields superior re-id matching accuracy than the state-of-the-art conventional supervised learning models, especially when the deployment gallery size becomes larger.

Hard Negative Mining As an effective scheme for improving model learning, negative mining has been extensively exploited in tackling computer vision problems, e.g. pedestrian detection [20], face recognition [60], image categorisation [28,51,78], and unsupervised visual representation learning [82]. Although hard negative samples are often collected automatically by deploying an up-to-date model with ground-truth labels, human verification

can provide an alternative approach to hard negative mining when ground-truth labels are unavailable [14]. In contrast to [14], HVIL has three significant advantages: (1) HVIL does not require pre-collected labelled training data. This is both necessary and critical for initialising the deep model of [14]. (2) HVIL requires only a handful of hard negative verifications from the top ranks, whereas a much larger number of human feedback is needed by [14] in order to have sufficient data for a deep model learning update. This makes HVIL much cheaper to be updated thus more scalable. (3) Due to the inherently costly training time for a deep model, it is infeasible for [14] to perform on-the-fly immediate model output update in responding to human feedback, losing the model effectiveness and cognitive benefit to the human in the loop. For person re-id, the recent POP model [44] also exploits hard negative mining by human verification. In comparison, the proposed HVIL human feedback protocol is simpler than that of POP, so that a user *only* focuses on the most salient negatives. This is more cost-effective than POP, as shown in our evaluation (Sec. 5.1).

Online Learning For learning from human feedback on-the-fly, the sequential and iterative model update in real-time poses an online learning problem [57]. In general, online learning algorithms have been widely applied in computer vision, especially for large-scale problems such as image retrieval [56,72], ranking [9], and classification [17]. Algorithmically, the proposed HVIL approach shares the principles of Passive-Aggressive (PA) online learning [13], where the learning objective has two terms: (1) A passive term that enforces the consecutively learned model parameter values to be close to each other at each time step, so to preserve the information learned from past data. (2) An aggressive term that encourages the model to incorporate information from new data. This enables the HVIL model to progressively cumulate knowledge from previous human feedback, therefore preserving human annotation effort and adapting to new data. Our experiments demonstrate its effectiveness (Sec. 3.2).

Interactive Learning Interactive model learning with human-in-the-loop is attractive for two reasons: (1) It provides a user with tools that can significantly alleviate or even eliminate the need for careful preparation of large-sized training data. (2) It allows to reduce the human labelling effort by exploiting a model’s capacity interactively. Human-computer interactive models have been considered in image segmentation [58,63], object recognition [8,71], semi-supervised clustering [36] and object counting [5]. In addition, relevance feedback [42,89,98] and active learning [27, 61] are also related to a similar idea of exploiting human feedback to improve model learning. The former has been exploited for interactive image retrieval where human feedback to search results

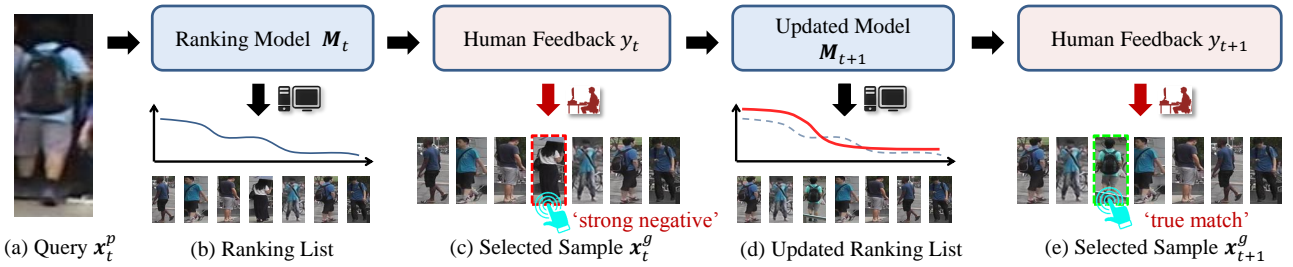


Fig. 4. Visualisation of the proposed Human-In-the-Loop person re-id procedure.

are used to refine a query. The latter aims to reduce the human labelling effort by active sample selection for model training. In active learning, knowledge cumulation during model deployment is not considered, and some offline pre-labelled data are typically needed for model initialisation.

Human-In-the-Loop Person Re-Id A small number of HIL re-id methods have been proposed recently. Abir et al. [15] (Fig. 3(b,c)) exploited human-in-the-loop verification to expand their multi-class based re-id model. Compared to HVIL, their method requires a pre-labelled training set for model initialisation. Another limitation is that such a model cannot generalise to new person classes re-id when human effort becomes unavailable. Hirzer et al. [26] (Fig. 3(d)) considered a form of human feedback which is ill-posed in practice: It only allows a user to verify whether a *true* match is within the top- k ranking list. This limits significantly the effectiveness of human feedback and can waste expensive human labour when a true match cannot be found in the top- k ranks, which is rather typical for a re-id model trained by small-sized training data and deployed to a larger-size test gallery population. More recently, Liu et al. [44] proposed the POP model (Fig. 2(d) and Fig. 3(d)), which allows a user to identify correct matches more rapidly and accurately by accommodating more flexible human feedback. However, POP requires to perform label propagation on an affinity graph over all gallery samples. This makes it poor for large gallery sizes (Sec. 5). Moreover, all existing HIL re-id models [15,26,44] do not benefit from cumulative learning, i.e. they treat each probe re-id as an independent modelling or retrieval task; therefore the process of model learning for re-id each probe does not benefit learning the models for other probes. This lack of improving model-learning cumulatively from increased human feedback is both suboptimal and disengaging the human in the loop. In contrast, the proposed HVIL re-id framework (Fig. 2(c) and Fig. 3(d)) enables incremental model improvement from cumulative human feedback thus maximising and encouraging human-machine interaction. Moreover, the proposed RMEL ensemble model further benefits from previous human verification effort to enable conventional HOL re-id tasks when human feedback is no long available. An earlier and preliminary version of this work was presented in [76]. Comparing to [76], this paper provides more detailed discussions, additional theoretical analysis, and more extensive evaluations.

3 HUMAN-IN-THE-LOOP INCREMENTAL LEARNING

3.1 Problem Formulation

Let a person image be denoted by a feature vector $\mathbf{x} \in \mathbb{R}^d$. The *Human-In-the-Loop (HIL) re-id* problem is formulated as: **(1)** For each image \mathbf{x}^p in a probe set $\mathcal{P} = \{\mathbf{x}_i^p\}_{i=1}^{N_p}$ (Fig. 4(a)), \mathbf{x}^p is matched against a gallery set $\mathcal{G} = \{\mathbf{x}_i^g\}_{i=1}^{N_g}$ and an initial ranking

list for all gallery images is generated by a re-id ranking function $f(\cdot) : \mathbb{R}^d \rightarrow \mathbb{R}$, according to ranking scores $f_{\mathbf{x}^p}(\mathbf{x}_i^g)$ (Fig. 4(b)). **(2)** A human operator (user) browses the gallery ranking list to verify the existence and the rank of any true match for \mathbf{x}^p . Human feedback is generated when a ranked gallery image \mathbf{x}^g is selected by the user with a label $y \in \{\text{true}, \text{dissimilar}\}$ (Fig. 4(c)). Once a feedback for probe \mathbf{x}^p is received, the parameters of re-id model $f(\cdot)$ are updated instantly (Fig. 4(d)) to re-order the gallery ranking list and give the user immediate reward for the next feedback (Fig. 4(e)). **(3)** When either a true match is found or a pre-determined maximum round of feedback is reached, the next probe is presented for re-id matching in the gallery set. In contrast to pre-labelling training data required by the conventional train-once-and-deploy *human-out-of-the-loop (HOL) re-id* scheme, *HIL re-id* has two unique characteristics: (a) Due to limited human patience and labour budget [26], a user typically prefers to examine only the top ranks rather than the whole rank list, and to provide only a few feedback. (b) Instead of seeking to verify *positives* (true matches) for each probe, which are most *unlikely* to appear in the top ranks¹, it is a much easier and more rewarding task for the user to identify *strong-negatives*, that is, those top ranked negative gallery instances “*definitely not the one I am looking for*” – visually very *dissimilar* to the target image.

Note that, in contrast to [44,76], here we consider a simpler human verification task by also ignoring *weak-negatives*: Those top ranked negative instances which “*look similar but not the same person as I am looking for*”. The reasons are: **(1)** A user is inclined to notice strong negatives among the top ranks, i.e. a cognitively easier task (Fig. 3(d)) due to that most top ranks are likely to be weak negatives. Making correct selection and verification of weak negatives requires much more effort. In contrast, a strong negative “pops out” readily to a user’s attention among the top ranks given the salience-driven visual selective attention mechanism built into the human visual system [54]. **(2)** We consider strong negatives in top ranks are *hard-unexpected negatives*: “Hard” since they are top-ranked negatives in the gallery thus misclassified with high confidence (short matching distance) to the wrong identity class by the current model; “Unexpected” since they are visually significantly dissimilar to the probe image whilst among the top ranks, therefore violating expectation and providing most informative feedback on model mistakes². Exploiting strong negatives to rectify model learning is more cost-effective with less labelling required (Sec. 5). Moreover, this is also compatible with the notion of salience-guided human eye movements therefore more likely to

1. In a large size gallery set, true matches are often scarce (only one-shot or few shots) and overwhelmed (appear in low-ranks) by false matches of high-ranks in the rank list.

2. In this context, weak negatives in top ranks can be considered as *hard-unexpected negatives* [14].

encourage a user to engage with the re-id task at hand whilst giving feedback, providing a higher degree of complementary effect between machine incremental learning from human feedback and human instant rewards from improved model output.

3.2 Modelling Human Feedback as a Loss Function

Formally, we wish to construct an incrementally optimised ranking function, $f_{\mathbf{x}^p}(\mathbf{x}_i^g) : \mathbb{R}^d \rightarrow \mathbb{R}$, where $f(\cdot)$ can be estimated by two types of human feedback $y \in L = \{m, s\}$ as *true-match* and *strong-negative* respectively. Inspired by [41,68,84], we define a ranking error (loss) function for a feedback y on a human selected gallery sample \mathbf{x}^g given a probe \mathbf{x}^p as:

$$\text{err}(f_{\mathbf{x}^p}(\mathbf{x}^g), y) = \mathcal{L}_y(\text{rank}(f_{\mathbf{x}^p}(\mathbf{x}^g))), \quad (1)$$

where $\text{rank}(f_{\mathbf{x}^p}(\mathbf{x}^g))$ denotes the rank of \mathbf{x}^g given by $f_{\mathbf{x}^p}(\cdot)$, defined as:

$$\text{rank}(f_{\mathbf{x}^p}(\mathbf{x}^g)) = \sum_{\mathbf{x}_i^g \in \mathcal{G} \setminus \mathbf{x}^g} \mathcal{I}(f_{\mathbf{x}^p}(\mathbf{x}_i^g) \geq f_{\mathbf{x}^p}(\mathbf{x}^g)), \quad (2)$$

where $\mathcal{I}(\cdot)$ is the indicator function. The loss function $\mathcal{L}_y(\cdot) : \mathbb{Z}^+ \rightarrow \mathbb{R}^+$ transforms a rank into a loss. We introduce a novel re-id ranking loss defined as:

$$\mathcal{L}_y(k) = \begin{cases} \sum_{i=1}^k \alpha_i, & \text{if } y \in \{m\} \\ \sum_{i=k+1}^{n_g} \hat{\alpha}_i, & \text{if } y \in \{s\} \end{cases}, \quad (3)$$

with $\alpha_1 \geq \alpha_2 \geq \dots \geq 0$, and $\hat{\alpha}_{n_g} \geq \hat{\alpha}_{n_g-1} \geq \dots \geq 0$.

Note, different choices of $\alpha_i, \hat{\alpha}_i$ lead to distinct model responses to human feedback (Fig. 5). We set $\alpha_i = \frac{1}{i}$ (large penalty with steep slope) when y indicates a *true-match* (m), and $\hat{\alpha}_i = \frac{1}{n_g - i + 1}$ with n_g the gallery size (small penalty with gentle slope) when y represents a *strong-negative* (s). Such a ranking loss is designed to favour a model update behaviour so that: (1) *true-matches* are quickly pushed up to the top ranks, whilst (2) *strong-negatives* are mildly moved towards the bottom rank direction. Our experiments (Sec. 5.1) show that such a ranking loss criterion boosts very effectively the Rank-1 matching rate and pushes quickly *true-matches* to the top ranks at each iteration of human feedback.

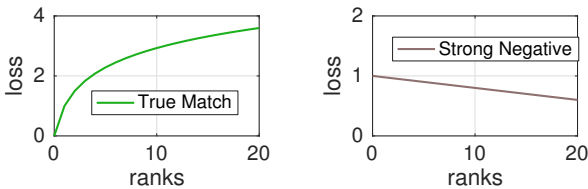


Fig. 5. Values of $\mathcal{L}_y(k)$ for distinct human feedback, with $n_g = 50$.

3.3 Real-Time Model Update for Instant Feedback Reward

Model Formulation Given the re-id ranking loss function defined in Eqn. (3), we wish to have real-time model update to human feedback therefore providing instant reward to user labour effort. To that end, we consider the HVIL re-id ranking model $f(\cdot)$ as a negative Mahalanobis distance metric:

$$f_{\mathbf{x}^p}(\mathbf{x}^g) = - \left[(\mathbf{x}^p - \mathbf{x}^g)^\top \mathbf{M} (\mathbf{x}^p - \mathbf{x}^g) \right], \quad \mathbf{M} \in S_+^d. \quad (4)$$

The positive semi-definite matrix \mathbf{M} consists of model parameters to be learned from sequential human feedback.

Knowledge Cumulation by Online Learning In the previous works [26,44], a re-id model $f(\cdot)$ is only optimised in isolation

for each probe without benefiting from previous feedback on other probes. To overcome this limitation, we wish to optimise $f(\cdot)$ *incrementally* in an online manner [9] for maximising the value of limited human feedback labour budget. Moreover, to achieve real-time human-in-the-loop feedback and reward, $f(\cdot)$ needs be estimated immediately on each human feedback.

Formally, given a new probe \mathbf{x}_t^p at time step $t \in \{1, \dots, \tau\}$ (τ the pre-defined verification budget), a user is presented with a gallery rank list computed by the previously estimated model \mathbf{M}_{t-1} instead of a new ranking function re-initialised from scratch for this new probe. The user then verifies a gallery image \mathbf{x}_t^g in the top ranks with a label y_t , generating a labelled triplet $(\mathbf{x}_t^p, \mathbf{x}_t^g, y_t)$. Given Eqn. (3), this triplet has a corresponding loss as $\mathcal{L}^{(t)} = \mathcal{L}_{y_t}(\text{rank}(f_{\mathbf{x}_t^p}(\mathbf{x}_t^g)))$. We update the ranking model by minimising the following object function:

$$\mathbf{M}_t = \underset{\mathbf{M} \in S_+^d}{\text{argmin}} \Delta_F(\mathbf{M}, \mathbf{M}_{t-1}) + \eta \mathcal{L}^{(t)}, \quad (5)$$

where Δ_F is a Bregman divergence measure, defined by an arbitrary differentiable convex function F , for quantifying the discrepancy between \mathbf{M} and \mathbf{M}_{t-1} . The set S_+^d defines a positive semi-definite (PSD) cone. The tradeoff parameter $\eta > 0$ balances the model update divergence and empirical ranking loss. This optimisation updates the ranking model adopted from the previous probe by encoding user feedback on the current probe.

Loss Approximation for Real-Time Optimisation In order to encourage and maintain user engagement in verification feedback, real-time online incremental metric learning is required. However, as $\mathcal{L}^{(t)}$ is discontinuous, the overall objective function cannot be optimised efficiently by gradient-based learning methods. We thus approximate the loss function by a continuous upper bound [41] so that it is differentiable w.r.t. the parameter \mathbf{M} :

$$\tilde{\mathcal{L}}^{(t)} = \frac{1}{\mathcal{N}_t^-} \sum_{\mathbf{x}_i^g \in \mathcal{G} \setminus \mathbf{x}_t^g} \mathcal{L}_{y_t} \left(\text{rank} \left(f_{\mathbf{x}_t^p}(\mathbf{x}_i^g | \mathbf{M}_{t-1}) \right) \right) \cdot h_{y_t} \left(f_{\mathbf{x}_t^p}(\mathbf{x}_i^g | \mathbf{M}_t) - f_{\mathbf{x}_t^p}(\mathbf{x}_i^g | \mathbf{M}_{t-1}) \right)^2, \quad (6)$$

where $f_{\mathbf{x}_t^p}(\mathbf{x}_i^g | \mathbf{M}_{t-1})$ denotes the function value of $f_{\mathbf{x}_t^p}(\mathbf{x}_i^g)$ parametrised by \mathbf{M}_{t-1} , and $h_{y_t}(\cdot)$ represents a hinge loss function defined as:

$$h_{y_t}(f_{\mathbf{x}_t^p}(\mathbf{x}_i^g) - f_{\mathbf{x}_t^p}(\mathbf{x}_i^g)) = \begin{cases} \max(0, 1 - f_{\mathbf{x}_t^p}(\mathbf{x}_i^g) + f_{\mathbf{x}_t^p}(\mathbf{x}_i^g)), & \text{if } y_t \in \{m\} \\ \max(0, 1 - f_{\mathbf{x}_t^p}(\mathbf{x}_i^g) + f_{\mathbf{x}_t^p}(\mathbf{x}_i^g)), & \text{if } y_t \in \{s\} \end{cases}. \quad (7)$$

The normaliser \mathcal{N}_t^- in Eqn. (6) is the amount of violators, i.e. the gallery instances that generate non-zero hinge loss (Eqn. (7)) w.r.t. the triplet $(\mathbf{x}_t^p, \mathbf{x}_i^g, y_t)$.

Learning Speed-up by Most Violator Update Given the loss approximation in Eqn. (6), we can exploit the stochastic gradient descent (SGD) algorithm [6] for optimising the proposed model objective function Eqn. (5) by iteratively updating on sub-sampled batches of all violators. However, the computational overhead of iterative updates can be high due to possibly large number of violators, and thus not meeting the real-time requirement. To address this problem, we explore a *most violator update* strategy, that is, to perform metric updates using *only* the violator \mathbf{x}_i^g with

the most violation (Eqn. (7)). The final approximated empirical loss is then estimated as:

$$\begin{aligned} \tilde{\mathcal{L}}_v^{(t)} &= \mathcal{L}_{y_t} \left(\text{rank}(f_{\mathbf{x}_t^g}(\mathbf{x}_t^g | \mathbf{M}_{t-1})) \right) \\ &\quad \cdot h_{y_t} \left(f_{\mathbf{x}_t^p}(\mathbf{x}_t^g | \mathbf{M}_t) - f_{\mathbf{x}_t^p}(\mathbf{x}_v^g | \mathbf{M}_{t-1}) \right)^2. \end{aligned} \quad (8)$$

Next, we derive \mathbf{M}_t for updating the ranking metric. Specifically, recall that the Bregman divergence between any two matrices \mathbf{A} and \mathbf{B} is defined as:

$$\Delta_F(\mathbf{A}, \mathbf{B}) = F(\mathbf{A}) - F(\mathbf{B}) - \text{tr}((\mathbf{A} - \mathbf{B})g(\mathbf{B})^\top), \quad (9)$$

where $g(\cdot)$ denotes the derivative of F (Eqn. (5)) [66] and $\text{tr}(\cdot)$ the matrix trace norm. After taking the gradient with the first argument \mathbf{A} , it has the following form:

$$\nabla_{\mathbf{A}} \Delta_F(\mathbf{A}, \mathbf{B}) = g(\mathbf{A}) - g(\mathbf{B}), \quad (10)$$

By replacing $\mathcal{L}^{(t)}$ in Eqn. (5) with $\tilde{\mathcal{L}}_v^{(t)}$, and setting the gradient of the minimisation objective in Eqn. (5) to zero, we have:

$$g(\mathbf{M}_t) - g(\mathbf{M}_{t-1}) + \eta \nabla_{\mathbf{M}} \tilde{\mathcal{L}}_v^{(t)} = 0. \quad (11)$$

This gives the following ranking metric online updating criterion:

$$\mathbf{M}_t = g^{-1} \left(g(\mathbf{M}_{t-1}) - \eta \nabla_{\mathbf{M}} \tilde{\mathcal{L}}_v^{(t)} \right), \quad (12)$$

where the gradient of $\tilde{\mathcal{L}}_v^{(t)}$ w.r.t. \mathbf{M} can be calculated as:

$$\nabla_{\mathbf{M}} \tilde{\mathcal{L}}_v^{(t)} = \hat{\mathcal{L}}(f_t - f_v - b_t) \mathbf{z}_t \mathbf{z}_t^\top, \quad (13)$$

with

$$\hat{\mathcal{L}} = \mathcal{L}_{y_t} \left(\text{rank}(f_{\mathbf{x}_t^p}(\mathbf{x}_t^g | \mathbf{M}_{t-1})) \right), \quad f_v = f_{\mathbf{x}_t^p}(\mathbf{x}_v^g | \mathbf{M}_{t-1}), \quad (14)$$

$$f_t = f_{\mathbf{x}_t^p}(\mathbf{x}_t^g | \mathbf{M}_t), \quad \mathbf{z}_t = \mathbf{x}_t^p - \mathbf{x}_t^g, \quad b_t = \begin{cases} 1, & \text{if } y_t \in \{m\}. \\ -1, & \text{if } y_t \in \{s\}. \end{cases}$$

For the convex function $F(\cdot)$, existing common choices include squared Frobenius norm $\|\mathbf{M}\|_F^2$ and quantum entropy $\text{tr}(\mathbf{M} \log(\mathbf{M}) - \mathbf{M})$. The incremental update of the HVIL model by Eqn. (12) can be then optimised by a standard gradient-based learning scheme such as [30,41,66]. In this work, we adopt a strictly convex function $F(\mathbf{M}) = -\log \det(\mathbf{M})$. This is because its gradient function $g(\cdot)$ is as simple as

$$g(\mathbf{M}) = \nabla_{\mathbf{M}} F(\mathbf{M}) = \mathbf{M}^{-1}, \quad (15)$$

and along with Eqn. (13) we can simplify Eqn. (12) as:

$$\mathbf{M}_t = \left(\mathbf{M}_{t-1}^{-1} - \eta \hat{\mathcal{L}}(f_t - f_v - b_t) \mathbf{z}_t \mathbf{z}_t^\top \right)^{-1}. \quad (16)$$

Applying the Sherman Morrison formula [85], we obtain the following online updating scheme for our HVIL model \mathbf{M} :

$$\mathbf{M}_t = \mathbf{M}_{t-1} - \frac{\eta \hat{\mathcal{L}}(f_t - f_v - b_t) \mathbf{M}_{t-1} \mathbf{z}_t \mathbf{z}_t^\top \mathbf{M}_{t-1}}{1 + \eta \hat{\mathcal{L}}(f_t - f_v - b_t) \mathbf{z}_t^\top \mathbf{M}_{t-1} \mathbf{z}_t} \quad (17)$$

To compute \mathbf{M}_t , we need to obtain the value of f_t which however is parametrised by \mathbf{M}_t (Eqn. (14)) and thus cannot be computed readily. One potential optimisation option is resorting to gradient approximation [17]. Instead, we propose to solve \mathbf{M}_t with exact gradient for more accurate modelling, inspired by the LEGO

metric update [29]. Specifically, by left multiplying \mathbf{M}_t with \mathbf{z}^\top and right multiplying with \mathbf{z} , we obtain

$$\mathbf{z}^\top \mathbf{M}_t \mathbf{z} = f_t = \frac{\hat{f}}{1 + \eta \hat{\mathcal{L}}(f_t - f_v - b_t) \hat{f}} \quad (18)$$

with $\hat{f} = f_{\mathbf{x}_t^p}(\mathbf{x}_t^g | \mathbf{M}_{t-1})$. Then, f_t can be solved by algebra transformation as:

$$f_t = \frac{\eta \hat{\mathcal{L}}(f_v + b_t) \hat{f} - 1 + \sqrt{(\eta \hat{\mathcal{L}}(f_v + b_t) \hat{f} - 1)^2 + 4\eta \hat{\mathcal{L}} \hat{f}^2}}{2\eta \hat{\mathcal{L}} \hat{f}} \quad (19)$$

Given this explicitly calculated f_t , we can evaluate quantitatively Eqn. (17) for online HVIL model updating. An overview of the HVIL online learning process is given in Algorithm 1. The updating scheme as described herein is favourable because it requires no computationally expensive eigen-decomposition to project the updated metric back to the PSD cone, and the positive definiteness of \mathbf{M}_t can be automatically guaranteed according to: **Theorem 1.** If \mathbf{M}_{t-1} is positive definite, then \mathbf{M}_t computed by Eqn. (17) is also positive definite.

Proof. If \mathbf{M}_{t-1} is a positive definite matrix, then

$$\hat{f} = f_{\mathbf{x}_t^p}(\mathbf{x}_t^g | \mathbf{M}_{t-1}) = \mathbf{z}_t^\top \mathbf{M}_{t-1} \mathbf{z}_t > 0 \quad \text{for all } \mathbf{z}_t.$$

Since $\eta > 0$, $\hat{\mathcal{L}} > 0$, we have

$$\sqrt{(\eta \hat{\mathcal{L}}(f_v + b_t) \hat{f} - 1)^2 + 4\eta \hat{\mathcal{L}} \hat{f}^2} > |\eta \hat{\mathcal{L}}(f_v + b_t) \hat{f} - 1|.$$

Therefore, from Eqn. (19) we have

$$f_t = f_{\mathbf{x}_t^p}(\mathbf{x}_t^g | \mathbf{M}_t) = \mathbf{z}_t^\top \mathbf{M}_t \mathbf{z}_t > 0 \quad \text{for all } \mathbf{z}_t.$$

Hence \mathbf{M}_t is also a positive definite matrix.

Model Complexity This online HVIL model update by Eqn. (17) is solved with a computational complexity of $\mathcal{O}(d^2)$ where d is the feature vector dimension, while a cost of $\mathcal{O}(d^3)$ is required by most other schemes which perform the Bregman projection back to the PSD cone [30,41,66]. Given all the components described above, our final model for Human Verification Incremental Learning (HVIL) enables real-time incremental model learning with human-in-the-loop feedback to model re-id rank list. As shown in our evaluation (Sec. 5.1), the proposed HVIL model provides faster human-in-the-loop feedback-reward cycles as compared to alternative models.

Algorithm 1: Human Verification Incremental Learning (HVIL)

Input: Unlabelled probe set \mathcal{P} and gallery set \mathcal{G} ;

Output: Per probe optimised ranking lists; re-id models $\{\mathbf{M}_t\}_{t=1}^\tau$;

1 **Initialisation:** $\mathbf{M}_0 = \mathbf{I}$ (identity matrix, equivalent to the L_2 distance)

2 **HIL person re-id:**

3 **while** $t < \tau$ **do**

4 Present the next probe $\mathbf{x}_t^p \in \mathcal{P}$;

 // `maxIter`: maximum interactions per probe

5 **for** $iter = 1 : \text{maxIter}$ **do**

6 Rank \mathcal{G} with \mathbf{M}_{t-1} against the probe \mathbf{x}_t^p (Eqn. (4));

7 Request the human feedback (\mathbf{x}_t^g, y_t) ;

8 Calculate $\tilde{\mathcal{L}}_v^{(t)}$ with the most violator \mathbf{x}_t^g (Eqn. (7) and (8));

9 $\mathbf{M}_t = \text{update}(\mathbf{M}_{t-1}, \tilde{\mathcal{L}}_v^{(t)})$ (Eqn. (12));

10 **Return** $\{\mathbf{M}_t\}_{t=1}^\tau$.

4 METRIC ENSEMBLE FOR HOL RE-ID

Finally, we consider the situation when the limited human labour budget is exhausted at time τ and an automated HOL re-id strategy is required for any further probes as in conventional approaches. In this setting, given that the HVIL re-id model is optimised incrementally during the HIL re-id procedure, the latest model \mathbf{M}_τ optimised by the human verified probe at time τ can be directly deployed. However, it is desirable to construct an even “stronger” model based on metric ensemble learning. Specifically, a side-product of HVIL is a series of models incrementally optimised *locally* for a set of probes with human feedback. We consider them as a set of *globally* “weak” models $\{\mathbf{M}_j\}_{j=1}^\tau$, and wish to construct a *single globally strong model* for re-identifying further probes without human feedback.

Regularised Metric Ensemble Learning Given weak models $\{\mathbf{M}_j\}_{j=1}^\tau$, we compute a distance vector $\mathbf{d}_{ij} \in \mathbb{R}^\tau$ for any probe-gallery pair $(\mathbf{x}_j^g, \mathbf{x}_i^p)$:

$$\mathbf{d}_{ij} = - \left[f_{\mathbf{x}_i^p}(\mathbf{x}_j^g | \mathbf{M}_1), \dots, f_{\mathbf{x}_i^p}(\mathbf{x}_j^g | \mathbf{M}_\tau) \right]^\top \quad (20)$$

The objective of metric ensemble learning is to obtain an optimal combination of these distances for producing a single globally optimal distance. Here we consider the ensemble ranking function $f_{\mathbf{x}_i^p}^{ens}(\mathbf{x}_j^g)$ in a bi-linear form (shortened as f_{ij}^{ens}):

$$f_{ij}^{ens} = f_{\mathbf{x}_i^p}^{ens}(\mathbf{x}_j^g) = -\mathbf{d}_{ij}^\top \mathbf{W} \mathbf{d}_{ij}, \quad \text{s.t. } \mathbf{W} \in S_+^\tau, \quad (21)$$

with \mathbf{W} being the ensemble model parameter matrix that captures the correlations among all the weak model metrics. In this context, previous work such as [52] is a special case of our model when \mathbf{W} is restricted to be diagonal only.

Objective Function To estimate an optimal ensemble weights \mathbf{W} with maximised identity-discriminative power, we re-use the true matching pairs verified during the human verification procedure (Sec. 3) as “training data”: $\mathcal{X}_{tr} = \{(\mathbf{x}_i^p, \mathbf{x}_i^g)\}_{i=1}^{N_t}$, and their corresponding person identities are denoted by $\mathcal{C} = \{c_i\}_{i=1}^{N_t}$. Note, “training data” here are only for estimating the ensemble model weight, not for learning a distance metric. Since the ranking score f_{ij}^{ens} in Eqn. (21) is either negative or zero, we consider that in the extreme case, an *ideal* ensemble function f_{ij}^* should provide the following ranking scores:

$$f_{ij}^* = \begin{cases} 0, & \text{if } c_i = c_j, \\ -1, & \text{if } c_i \neq c_j. \end{cases} \quad (22)$$

Using \mathbf{F}^* to denote such an ideal ranking score matrix and \mathbf{F}^{ens} to denote an estimated score matrix by a given \mathbf{W} with Eqn. (21), our proposed objective function for metric ensemble learning is then defined as:

$$\rho = \min_{\mathbf{W}} \|\mathbf{F}^{ens} - \mathbf{F}^*\|_F^2 + \nu \mathcal{R}(\mathbf{W}), \quad \text{s.t. } \mathbf{W} \in S_+^\tau, \quad (23)$$

where $\|\cdot\|_F$ denotes a Frobenius norm, and $\mathcal{R}(\mathbf{W})$ a regulariser on \mathbf{W} with parameter ν controlling the regularisation strength. Whilst common choices of $\mathcal{R}(\mathbf{W})$ include L_1 , Frobenius norm, or matrix trace, we introduce the following regularisation for a Regularised Metric Ensemble Learning (RMEL) re-id model:

$$\mathcal{R}(\mathbf{W}) = - \sum_{i,j} f_{ij}^{ens}, \quad \text{if } c_i = c_j. \quad (24)$$

Our intuition is to impose severe penalties for true match pairs with low ranking scores since they deliver the most informative

discriminative information for cross-view person re-id, whilst false match pairs are less informative.

Optimisation Eqn. (23) is strictly convex with a guaranteed global optimal so it can be optimised by any off-the-shelf tool-boxes [24]. We adopt the standard first-order projected gradient descent algorithm [7], with the gradient of Eqn. (23) computed as:

$$\nabla_{\mathbf{W}} = \sum_{i,j} (f_{ij}^* - f_{ij}^{ens} + \nu \mathcal{I}[c_i = c_j]) \mathbf{d}_{ij} \mathbf{d}_{ij}^\top, \quad (25)$$

with \mathcal{I} being the indicator function. Our optimisation algorithm is summarised in Algorithm 2.

Algorithm 2: Regularised Metric Ensemble Learning (RMEL)

Input: Training dataset $\mathcal{X}_{tr} = \{(\mathbf{x}_i^p, \mathbf{x}_i^g)\}_{i=1}^{N_t}$, label set $\mathcal{C} = \{c_i\}_{i=1}^{N_t}$, learning rate ϵ , max learning iteration τ_{me} , and weak HVIL models $\{\mathbf{M}_j\}_{j=1}^\tau$;

Output: The optimal weight matrix \mathbf{W} for the metric ensemble;

- 1 **Initialisation:** Randomly initialise \mathbf{W}_0 to some PSD matrix.
 - 2 **Metric Ensemble Learning:**
 - 3 **for** $k = 1 : \tau_{me}$ **do**
 - 4 Calculate gradient $\nabla_{\mathbf{W}_{k-1}}$ (Eqn. (25));
 - 5 Set $\mathbf{W}_k = \mathbf{W}_{k-1} - \epsilon \nabla_{\mathbf{W}_{k-1}}$;
 - 6 Perform eigen-decomposition of \mathbf{W}_k : $\mathbf{W}_k = \sum_i \lambda_i \mathbf{u}_i \mathbf{u}_i^\top$;
 - 7 Project \mathbf{W}_k back to PSD cone:
 - 8 $\mathbf{W}_k = \sum_i \max(\lambda_i, 0) \mathbf{u}_i \mathbf{u}_i^\top$.
 - 9 **Return** \mathbf{W} .
-

HOL Person Re-Id Given the estimated optimal ensemble weight matrix \mathbf{W} and the weak models $\{\mathbf{M}_j\}_{j=1}^\tau$, a single strong ensemble model (Eqn. (21)) is made available for performing automated HOL re-id of any further probes on the gallery population. Our experiments (Sec. 5.2) show that the proposed RMEL algorithm achieves superior performance as compared to state-of-the-art supervised re-id models given the same amount of labelled data.

5 EXPERIMENTS

Two sets of comparative experiments were conducted: (1) The proposed HVIL model was evaluated under a *Human-In-the-Loop* (HIL) re-id setting and an *enlarged* test gallery population was used to reflect real-world use-cases (Sec. 5.1). (2) In the event of limited human labour budget being exhausted and human feedback becoming unavailable, the proposed HVIL-RMEL model was evaluated under an automated *human-out-of-the-loop* (HOL) re-id setting (Sec. 5.2).

Datasets Two largest person re-id benchmarks: CUHK03 [38] and Market-1501 [95], were chosen for evaluations due to the need for large test gallery size. CUHK03 contains 13,164 bounding box images of 1,360 people. Two versions of person image are provided: manually labelled and automatically detected, with the latter presenting more realistic detection misalignment challenges for practical deployments (Fig. 6(a)). We used both. Market-1501 has 32,668 person bounding boxes of 1,501 people, obtained by automatic detection. Both datasets cover six outdoor surveillance cameras with severely divergent and unknown viewpoints, illumination conditions, (self)-occlusion and background clutter (Fig. 6(b)). In addition, we also selected the most common benchmark VIPeR [25] characterised with low imaging resolution and dramatic illumination variations (Fig. 6(c)). Compared to CUHK03 and Market-1501, VIPeR has a much smaller population size (632 people) with fewer (1,264) labelled person images, therefore



Fig. 6. Examples of cross-view person images from three person re-id datasets. Two images in each column describe the same person.

only suitable for the conventional HOL re-id setting. These three datasets present a wide range of re-id evaluation challenges under different viewing conditions and with different population sizes, as summarised in Table 1.

TABLE 1
Settings of three person re-id datasets.

Dataset	Cams	IDs	Labelled	Detected	HIL Split	HOL Split
VIPeR [25]	2	632	1,264	0	-	316/316
CUHK03 [38]	6	1,467	13,164	13,164	1,000	360
Market-1501 [95]	6	1,501	0	32,668	1,000	501

Data Partitions For CUHK03 or Market-1501, we randomly selected 1,000 identities D_{p1} (p stands for population) as the partition to perform *HIL* re-id experiments. The remaining partition of people D_{p2} (360 on CUHK03, and 501 on Market-1501) were separated for evaluating the proposed model against state-of-the-art supervised re-id methods for automated *HOL* re-id (see details in Sec. 5.1 and Sec. 5.2). Due to its small size, VIPeR was only used in the *HOL* experiments and the identities were split half-half for training and testing. To obtain statistical reliability, we generated 10 different trials with different random partitions and reported their averaged results.

Visual Features We adopted two types of image features: **(1)** The WHOS descriptor [43]: A state-of-the-art *hand-designed* person re-id feature (5,138 dimensions) composited by colour, HOG [83] and LBP [3] histograms extracted from horizontal rectangular stripes³. **(2)** The CNN feature learned by a recently proposed deep architecture for re-id [21]: In contrast to hand-crafted WHOS features, deep CNN features are extracted from a deep model trained by supervised learning from a large number of labelled training data. Specifically, we trained the deep model with the entire person search dataset [87], which is independent of CUHK03, Market-1501 and VIPeR, therefore without any additional effect on their data partitions. The trained deep model is directly deployed as a feature extractor (1,024 dimensions) without any domain transfer learning by fine-tuning on the three evaluation datasets. Whilst adopting deep features from training a CNN model using labelled data may seem to be inconsistent with the objective of this work – eliminating the need for offline pre-collected training data, the main purposes of utilising the CNN feature are: (a) To evaluate the proposed HVIL on different features; (b) To demonstrate any additional benefit of the proposed HVIL model on a strong deep feature already learned from a large size labelled training data.

Evaluation Metrics We adopted three performance evaluation metrics in the following experiments: (1) Cumulative Match

3. The LOMO (26,960 dimensions) [39] and GOG (27,622 dimensions) [49] were not selected due to their high dimensionality property which poses high computational cost for online model updating, although they are possibly more discriminative.

Characteristic (CMC): calculated as the cumulative recognition rate at each rank position. (2) Expected Rank (ER): defined as the average rank of all true matches. (3) Mean Average Precision (mAP): first computing the area under the Precision-Recall curve for each probe, then calculating the mean of Average Precision over all probes. For all *HIL* re-id models, we used the ranking result after the final human feedback applied on each probe. The averaged results over all 10 trials were reported in comparisons.

5.1 Human-In-the-Loop Re-Id Evaluations

5.1.1 Experiment Settings

Probe/Gallery Configuration For each of the D_{p1}^i partitions, we built a probe set for human operators to perform *HIL* re-id. In each trial, the probe set \mathcal{P}^i contains randomly selected 300 persons with one image per person. For building the cross-view gallery set, we considered three different configurations to fully analyse the behaviour and scalability of the proposed HVIL method: **(1) Single-shot gallery \mathcal{G}_s^i** : We randomly selected one cross-view image per person of all the 1,000 identities in partition D_{p1}^i and construct a single-shot gallery set \mathcal{G}_s^i (1,000 person images) on both CUHK03 and Market-1501. **(2) Multi-shot gallery \mathcal{G}_m^i** : We built the multi-shot gallery \mathcal{G}_m^i by following [95]. In particular, for all the 1,000 identities in partition D_{p1}^i , we used all cross-view images to construct the gallery set. As such, the average gallery image number is 4,919 on CUHK03 and 9,065 on Market-1501. Note that, we did not utilise the label information about which gallery images are of the same person, and thus both CMC and mAP can be used for performance evaluation. **(3) Open-world gallery \mathcal{G}_d^i** : We considered a more challenging setting with a large number of distractors involved in the gallery set. Specifically, we added 34,574 bounding boxes of 11,934 persons from the person search dataset [87] to the single-shot gallery set \mathcal{G}_s^i . The resulted gallery \mathcal{G}_d^i size is 35,574 on both datasets. This is to evaluate the scalability of *HIL* re-id methods when operating under the open-world re-id setting featured with a huge gallery search space.

Human Feedback Protocol Human feedback were collected on all 10 trials of D_{p1}^i partitions and all 3 different gallery configurations, in total $3 \times 10 = 30$ independent sessions on each dataset by 5 volunteers as users. During each session, a user was asked to perform the *HIL* re-id on probes in the probe set \mathcal{P}^i against a gallery set $\mathcal{G}^i \in \{\mathcal{G}_s^i, \mathcal{G}_m^i, \mathcal{G}_d^i\}$. For each probe person, a *maximum* of 3 rounds of user interactions are allowed. We limited the users to verify only the top-50 in the rank list (5% of \mathcal{G}_s^i , 0.5 ~ 1% of \mathcal{G}_m^i , and 0.1% of \mathcal{G}_d^i). During each interaction: (1) A user selects one gallery image as either *strong-negative* or *true-match*; and (2) the system takes the feedback, updates the ranking function and returns the re-ordered ranking list, all in real-time (Sec. 3). The HVIL model was evaluated against ten existing models for *HIL* re-id deployment as follows.

HIL Competitors Three existing *HIL* models were compared: (1) POP [44]: The current state-of-the-art *HIL* re-id method based on Laplacian SVMs and graph label propagation; (2) Rocchio [42]: A probe vector modification model updates iteratively the probe’s feature vector based on human feedback, widely used for image retrieval tasks [16]; (3) EMR [89]: A graph-based ranking model that optimises the ranking function by least square regression. For a fair comparison of all four *HIL* models, the users were asked to verify the same probe and gallery data ($\mathcal{P}^i, \mathcal{G}^i$) with the same two types of feedback given the ranking-list generated by each model.

TABLE 2

Human-in-the-loop person re-id with **single-shot** galleries. Gallery Size: 1,000 for both CUHK03 and Market-1501. **L**: Labelled; **D**: Detected.

Feature	WHOS [43]									CNN [21] (except for DGD and Inception-V3)								
	CUHK03 (L)			CUHK03 (D)			Market-1501 (D)			CUHK03 (L)			CUHK03 (D)			Market-1501 (D)		
	Rank (%)	1	50	100	1	50	100	1	50	100	1	50	100	1	50	100	1	50
L2	2.9	31.1	43.2	2.7	29.8	41.6	16.1	66.6	76.6	19.0	72.0	82.3	17.1	67.0	78.1	44.2	94.4	97.5
kLFDA [88]	5.9	47.3	60.1	4.7	39.6	51.7	21.8	85.8	91.5	21.4	77.4	86.2	19.4	73.7	82.7	52.9	97.2	98.5
XQDA [39]	3.7	40.2	53.6	2.4	22.4	33.3	18.3	75.1	83.5	19.8	76.9	85.8	17.7	73.9	83.0	49.6	97.0	98.5
MLAPG [40]	4.2	39.5	52.4	3.5	36.1	49.3	24.1	84.5	91.2	11.8	69.6	82.5	10.2	64.3	77.9	37.7	95.5	97.9
NFST [91]	7.1	41.5	54.7	4.9	37.4	48.5	34.4	85.3	90.7	9.9	41.7	51.3	9.5	38.0	47.8	45.0	89.7	93.3
HER [75]	7.6	46.0	58.1	5.7	41.8	53.8	39.1	90.8	94.7	16.2	73.5	84.3	14.5	69.9	80.2	44.0	96.1	98.3
DGD [86]	-	-	-	-	-	-	-	-	-	12.0	58.0	69.8	10.1	49.8	61.6	58.4	95.7	97.4
Inception-V3 [65]	-	-	-	-	-	-	-	-	-	15.7	63.7	74.4	15.3	62.5	72.2	51.6	94.7	96.8
EMR [89]	29.3	29.3	40.7	27.7	27.7	39.5	64.2	64.2	74.2	73.5	73.5	83.7	66.7	66.7	77.5	92.7	92.7	96.8
Rocchio [42]	32.0	38.7	46.2	29.0	36.2	43.8	61.7	70.2	77.5	62.0	79.2	85.2	56.2	74.3	80.8	81.2	94.5	93.3
POP [44]	44.0	51.5	60.0	41.7	48.5	58.8	75.0	78.5	84.5	74.7	74.8	77.2	69.0	70.7	73.2	92.8	93.0	93.3
HVIL (Ours)	60.2	68.2	78.5	53.7	65.0	75.3	84.5	89.2	93.2	84.2	89.2	93.3	80.3	86.0	91.2	95.3	96.0	98.3

TABLE 3

Human-in-the-loop person re-id with **multi-shot** galleries. Gallery Size: 4,919 for CUHK03 and 9,065 for Market-1501. **L**: Labelled; **D**: Detected.

Feature	WHOS [43]						CNN [21] (except for DGD and Inception-V3)					
	CUHK03 (L)		CUHK03 (D)		Market-1501 (D)		CUHK03 (L)		CUHK03 (D)		Market-1501 (D)	
	Rank (%)	R-1	mAP	R-1	mAP	R-1	mAP	R-1	mAP	R-1	mAP	R-1
L2	4.1	14.1	3.6	13.9	28.0	23.9	22.0	29.5	20.7	28.0	58.0	50.9
kLFDA [88]	8.1	17.8	6.3	16.5	47.1	39.9	25.4	32.8	23.9	31.0	67.7	63.0
XQDA [39]	3.6	14.9	4.5	14.5	34.3	30.1	24.5	31.7	22.5	30.0	63.4	58.1
MLAPG [40]	5.0	15.1	5.1	15.1	44.3	40.8	14.8	23.7	12.2	21.9	54.5	50.8
NFST [91]	8.2	17.5	7.7	16.6	68.3	62.1	20.2	26.8	18.6	25.3	76.2	69.9
HER [75]	9.5	18.6	8.1	17.4	68.9	61.7	24.3	31.4	22.3	29.3	77.4	72.1
DGD [86]	-	-	-	-	-	-	15.1	23.5	13.0	21.4	82.1	75.9
Inception-V3 [65]	-	-	-	-	-	-	19.2	27.1	18.3	26.2	76.3	71.4
EMR [89]	30.8	20.2	29.7	19.3	76.0	31.7	71.3	40.6	66.3	37.5	94.0	57.7
Rocchio [42]	34.0	26.4	30.7	23.7	74.3	37.1	59.3	50.0	56.0	46.8	83.7	65.1
POP [44]	43.0	39.4	44.3	38.2	82.7	52.7	71.7	68.2	68.0	64.3	94.0	74.0
HVIL (Ours)	63.0	59.0	53.7	48.7	87.3	63.3	84.0	73.4	80.7	72.7	96.0	83.3

HOL Competitors In addition, seven state-of-the-art conventional HOL supervised learning models were also compared: kLFDA [88], XQDA [39], MLAPG [40], NFST [91], HER [75], DGD [86], and Inception-V3 [65], among them two are deep learning models (DGD and Inception-V3). These supervised re-id methods were trained using fully pre-labelled data in the separate partition D_{p2}^i (CUHK03: averagely 3,483 images of 360 identities; Market-1501: averagely 7,737 images of 501 identities) before being deployed to \mathcal{P}^i and \mathcal{G}^i for automated HOL re-id testing. Note, the underlying human labour effort for pre-labelling the training data to learn these supervised models was significantly greater – exhaustively searching 3,483 and 7,737 *true* matched images respectively for CUHK03 and Market-1501, than that required by the HIL methods – between 300 to 900 *indicative* verification (strong negative or true match) given a maximum of 300 probes with each allocated a maximum of 3 feedback on both CUHK03 and Market-1501, so only 1/10th of and weaker user input than supervised HOL models. It should be noted that non-deep distance metric models (kLFDA, XQDA, MLAPG, NFST, HER) were trained using either hand-crafted WHOS [43] or deep learning CNN [21] features (Sec. 5), while DGD and Inception-V3 were trained directly from raw images in D_{p2}^i with the intrinsic capability of learning their own deep CNN features (256 dimensions for DGD and 2,048 for Inception-V3).

Implementation Details For implementing the HVIL model (Sec. 3), the only hyper-parameter η (Eqn. (5)) was set to 0.5 on both CUHK03 and Market-1501. We found that HVIL is insensitive to η with a wide satisfiable range from 10^{-1} to 10^1 . For POP, EMR, and Rocchio, we adopted the authors’ recommended parameter settings as in [42,44,89]. For all HIL methods above,

we applied L_2 distance as the initial ranking function $f_0(\cdot)$ without loss of generalisation⁴. Note that for HVIL, once $f_0(\cdot)$ was initialised for only the very first probe, it was then optimised incrementally across different probes. In contrast, for POP and EMR and Rocchio, each probe had its own $f_0(\cdot)$ initialised as L_2 since the models are not cumulative across different probes. For HOL competitors, the parameters were determined by cross-validation on D_{p2} with the authors’ published codes. All the models except DGD and Inception-V3 used the same two feature descriptors for comparison (WHOS [43] and CNN feature [21]). DGD [86] and Inception-V3 [65] used their own deep features from training their CNN networks.

5.1.2 Evaluations on Person Re-Id Performance

The person re-id performances of all HIL and HOL methods on \mathcal{P}^i and $\{\mathcal{G}_s^i, \mathcal{G}_m^i, \mathcal{G}_d^i\}$ are compared in Tables 2 (single-shot), 3 (multi-shot), and 4 (open-world) respectively.

HIL vs. HOL Re-Id Methods We first compared the re-id matching performance of HIL and HOL re-id schemes. It is evident from the three Tables that the HIL methods outperform significantly the conventional HOL counterparts in all testing settings on both datasets. Specifically, in single-shot setting (Table 2), *all* conventional supervised re-id models suffered severely when the gallery size was enlarged to 1,000 from their standard setting. For example, the state-of-the-art deep re-id model DGD [86] can achieve 72.6% Rank-1 rate on CUHK03 (Labelled) under the test protocol of using the 100-sized test gallery. However, its

⁴ No limitation on considering any other distance or similarity metrics, either learned or not. However, non-learning based generic metrics are more scalable and transferable in real-world.

TABLE 4

Human-in-the-loop person re-id with **open-world** galleries consisting of 34,574 **distractors**. Gallery Size: 35,574 for both CUHK03 and Market-1501. **L**: Labelled; **D**: Detected. Note: POP results are unavailable because it was *intractable* on our computing hardware.

Feature	WHOS [43]									CNN [21] (except for DGD and Inception-V3)								
	CUHK03 (L)			CUHK03 (D)			Market-1501 (D)			CUHK03 (L)			CUHK03 (D)			Market-1501 (D)		
Rank (%)	1	50	100	1	50	100	1	50	100	1	50	100	1	50	100	1	50	100
L2	2.8	27.2	38.2	2.6	24.8	34.4	10.7	43.9	51.5	18.3	69.6	80.1	16.6	65.0	75.9	31.4	77.6	84.0
kLFDA [88]	5.6	32.9	44.8	3.6	28.1	38.0	19.8	67.6	76.1	17.7	66.9	77.1	16.8	63.6	72.9	38.4	84.2	89.7
XQDA [39]	3.1	25.3	36.3	2.4	21.7	32.0	16.6	61.9	70.7	15.5	61.7	70.6	13.2	58.1	67.7	31.3	77.0	84.4
MLAPG [40]	3.7	33.3	44.0	2.8	28.9	39.2	18.9	67.6	76.3	6.4	34.6	43.1	5.8	30.2	37.9	20.1	65.0	74.0
NFST [91]	5.6	34.6	45.6	4.2	30.3	40.5	30.1	78.3	85.0	9.8	41.4	51.0	9.4	37.8	47.5	39.6	83.7	88.4
HER [75]	6.3	36.2	46.0	4.5	31.4	40.5	32.7	80.8	86.0	12.3	57.3	66.5	11.8	54.7	64.1	26.1	70.6	79.0
DGD [86]	-	-	-	-	-	-	-	-	-	7.2	29.1	35.0	5.6	23.2	29.0	48.6	86.3	89.2
Inception-V3 [65]	-	-	-	-	-	-	-	-	-	8.9	31.5	38.2	7.4	30.5	37.6	37.0	79.4	83.9
EMR [89]	25.8	25.8	35.5	23.1	23.1	32.2	40.8	40.8	46.8	70.7	70.7	81.0	66.3	66.3	77.7	72.7	72.7	80.7
Rocchio [42]	28.7	32.3	37.5	25.3	30.0	37.0	43.6	46.2	48.8	61.0	74.0	81.7	56.7	73.7	80.0	64.3	74.3	80.0
POP [44]	-	-	-	-	-	-	-	-	-	-	-	-	-	-	-	-	-	-
HVIL (Ours)	55.6	65.7	74.8	52.0	60.3	67.8	61.7	70.8	76.7	80.3	86.0	91.3	73.3	84.7	89.3	91.3	93.3	96.0

Rank-1 accuracy drops dramatically to only 12.0% Rank-1 on CUHK03 (Labelled) and 10.1% (Detected) under the 1,000-sized test gallery evaluated here. Similar performance drops occur for all other HOL models. Such low Rank-1 matching accuracies show that, existing best supervised re-id approaches are still far from being sufficiently mature to provide a fully automated HOL re-id solution in real world. On the contrary, HIL methods make more realistic assumptions by considering human in the loop, and leverage limited human efforts to directly drive up model matching performance by mining the joint human-machine benefits. The advantage in re-id matching by the HOL methods is clear: for example, with WHOS feature the proposed HVIL achieves over 50% and 80% in Rank-1 on CUHK03 and Market-1501 (Table 2), which is much more acceptable in practical use. In terms of supervision cost, the supervised HOL models were offline trained on a large-sized pre-labelled data in D_{p2} with an average of 3,483 cross-view images of 360 identities on CUHK03, and 7,737 images of 501 identities on Market-1501. Whereas the HIL models required much less human verification effort, e.g. at most 3 feedback for each probe in top-50 ranks only, in total 300 ~ 900 weak feedback. Human feedback is neither restricted to be only true matches, nor exhaustively labelling person identity labels, nor searching true matches in a huge image pool. These evidences suggest that HIL re-id is a more cost-effective and promising scheme in exploiting human effort for real-world applications as compared to the conventional HOL re-id approach.

Among all HIL re-id models, the proposed HVIL achieves the best performance. For instance, it is found in Table 2 that the HVIL improves significantly over the state-of-the-art HIL model POP on Rank-1 score, e.g. from 44.0% to 60.2% on CUHK03 (Labelled), from 41.7% to 53.7% on CUHK03 (Detected), and from 75.0% to 84.5% on Market-1501, when the WHOS feature is used. HVIL’s advantage continues over all ranks. This demonstrates the compelling advantages of the HVIL model in cumulatively exploiting human verification feedback, whilst other existing human-in-the-loop models have no mechanisms for sharing human feedback knowledge among different probes.

Effect of Features Next, we evaluated the effect of different visual features by comparing the hand-crafted WHOS [43] and the most recent deep CNN feature [21] learned from the large scale person search dataset [87]. As shown in Table 2, the CNN feature is much more discriminative and view-invariant than the WHOS thanks to the access of large quantity of labelled data and the strong deep representation learning capacity. Specifically,

with CNN feature, even the generic L2 metric can achieve 19.0%/17.1% and 44.2% on CUHK03 (Labelled/Detected) and Market-1501, respectively. Importantly, CNN feature can be well complementary with HIL re-id methods: The HIL re-id Rank-1 rates are further boosted to a more satisfying level, e.g. 84.2%/80.3% and 95.3% by the proposed HVIL. This implies the great compatibility of the HVIL with deep feature learning. On the other hand, it is found that with such a powerful deep CNN feature, HOL models are still outperformed drastically by HIL methods. This suggests the consistent and general advantages of the HIL re-id scheme over the HOL approach given various types of visual features.

Single-Shot vs. Multi-Shot We evaluated the effect of shot number in the gallery set in person re-id performance. When more shots of a person are available (Table 3 vs. Table 2), re-id matching accuracy can be improved in most cases by either HIL and HOL methods including the proposed HVIL. However, the best results are still generated by the HVIL model. This suggests the steady advantage of the proposed method in different search gallery settings. In particular, we have the following observations and justifications: (1) The Rank-1 improvement degree varies over different datasets, with Market-1501 benefiting more than CUHK03. The plausible reason is that, Market-1501 person images give more pose and detection misalignment challenge due to poorer person bounding box detection, and therefore multi-shot images with various poses and detection qualities can bring more gains. (2) The HVIL model seem to benefit less from multi-shot gallery images as compared to other methods. This may be due to the better capability of mitigating the pose/detection misalignment challenge by the proposed incremental model learning, thus not needing multiple shots as much as the other models do.

Effect of Distractors in Open-World Setting Finally, we evaluated the effect of open-world distractors in the gallery set for further testing the model scalability. This evaluation is made by comparing Table 2 and Table 4. After adding 34,574 person bounding boxes as distractors to the 1000 sized single-shot gallery (i.e. the gallery size is enlarged by 35 times), we observed that (1) As expected, all methods suffered from some drop in re-id performance; (2) The HIL methods outperform more significantly the HOL models under the open-world setting; and (3) the proposed HVIL again achieves the best re-id performance, and particularly on the CUHK03 (Detected) dataset, the addition of 34K distractors causes only a 1.7% = 53.7% - 52.0% Rank-1 drop. This again suggests the clear advantages and superiority of having human in

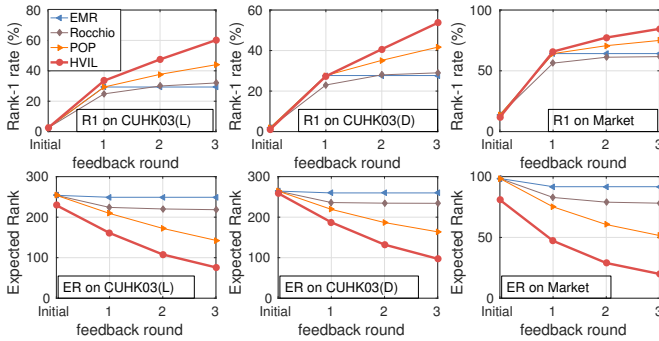


Fig. 7. Comparing Rank-1 score and Expected Rank (ER) on human feedback rounds.

the loop for real-world person re-id applications when the gallery population size is inevitably large in the open-world operation scenarios. More specifically, when the WHOS feature was used, the best HOL model HER’s Rank-1 rates dropped from 7.6% to 6.3%, 5.7% to 4.5%, and 39.1% to 32.7% on CUHK03 (Labelled), CUHK03 (Detected), and Market-1501 respectively. The best HIL competitor, POP, completely fails to operate with such a large gallery set. The reason is that POP requires to build an affinity graph and calculate the graph Laplacian on all the gallery samples to propagate human labels. Given a 34,574-sized gallery set, the affinity graph alone takes 4.78 GB storage which is both difficult to process (out of memory) for common workstations and suffering from slow label propagation.

5.1.3 Further Analysis on Human Verification

We examined the effectiveness of the proposed HVIL model in exploiting human verification effort for HIL re-id in the single-shot setting with the WHOS feature.

Statistics Analysis on Human Verification Fig. 7 shows the comparisons of Rank-1 and Expected Rank (ER) on the 4 human-in-the-loop models over three verification feedback rounds. It is evident that the proposed HVIL model is more effective than the other three models in boosting Rank-1 scores and pushing up true matches’ ranking orders. The reasons are: (1) Given a large gallery population with potentially complex manifold structure, it is difficult to perform accurately graph label propagation for graph-based methods like POP and EMR. (2) Unlike POP/EMR/Rocchio, the proposed HVIL model optimises on re-id ranking losses (Eqn. (3)) specifically designed to maximise the two types of human verification feedback. (3) The HVIL model enables knowledge cumulation (Eqn. (5)). This is evident in Fig. 7 where HVIL yields notably better (lower) Expected Ranks (ER), even for the initial ER before verification feedback takes place on a probe (due to benefiting cumulative effect on sequential human feedback from other probes). In contrast, other models do not improve initial ER on each probe due to the lack of a mechanism to cumulate experience on-the-fly.

Human Verification Cost-Effectiveness We further evaluated the human verification effort in relation to re-id performance benefit by analysing the meta statistics of HIL re-id experiments above. We compared the HVIL model with the POP model and Exhaustive Search (ES) where a user performs exhaustive visual searching over the whole gallery ranking list (1,000) generated by L2 metric until finding a true match. The averaged statistics over all 10 trials were compared in Table 5. It is evident that though ES is guaranteed to locate a true match for every probe if

TABLE 5
Human verification effort vs. benefit. All measures are from averaging over all probes. Setting: single-shot. Feature: WHOS. ↓: lower better; ↑: higher better. ES: Exhaustive Search.

Dataset	CUHK03 (L)		CUHK03 (D)		Market-1501 (D)				
	Method	HVIL POP ES	HVIL POP ES	HVIL POP ES	HVIL POP ES				
Found-matches(%) ↑	60.2	44.0	100	53.7	41.7	100	84.5	75.0	100
Browsed-images ↓	35.1	57.3	253.9	71.6	107.0	264.3	19.7	33.8	98.5
Feedback ↓	2.2	2.4	-	2.4	2.4	-	1.6	1.7	-
Search-time(sec.) ↓	23.5	47.3	187.0	33.0	55.8	234.9	14.7	22.7	131.8

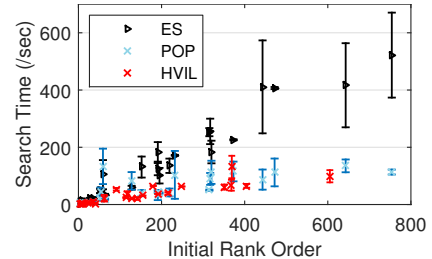


Fig. 8. Search time from different HIL models on the same 25 randomly selected probes. Dataset: CUHK03 (Labelled). Setting: single-shot.

it existed, it is much more expensive than POP (3×) and HVIL (5×) in search time given a 1,000-sized gallery. This difference will increase further on larger galleries. Comparing HVIL and POP, it is evident that HVIL is both more cost-effective (less Search-time, Browsed-images and Feedback) and more accurate (more Found-matches).

HIL Re-Id Search Speed To better understand model convergence given human feedback, we conducted a separate experiment to measure the search time by different human-in-the-loop models given the initial rank lists on 25 randomly selected probes verified by multiple users. This experiment was evaluated by 10 independent sessions with the same set of 25 probes provided. In each session, the users were required to find a true match for all 25 probes. Specifically, for HVIL and POP, if a true match was not identified after 3 (maximum) feedback, the users then performed an exhaustive searching until it was found. The search time statistics for all 25 probes are shown in Fig. 8, where a bar shows the variance between 10 different sessions. It is unsurprising that ES is the least efficient whilst HVIL is the quickest in finding a true match, i.e. the data points of HVIL are much lower in search time. Moreover, it is evident that HVIL yields much better initial ranks, i.e. the data points of HVIL are more centred towards the bottom-left corner. This further shows the benefit of cumulative learning in HVIL (Sec. 3.3).

TABLE 6
Effect of strong and weak negatives in HIL re-id performance.

Dataset	CUHK03 (L)		CUHK03 (D)		Market-1501 (D)	
	Metric	R1(%)	ER	R1(%)	ER	R1(%)
Strong	60.2	76.0	53.7	99.8	84.5	20.0
Weak	45.3	203.0	43.6	226.7	78.0	90.7

Strong vs. Weak Negatives We evaluated explicitly the effect of strong and weak negative feedback on the HIL re-id performance. To this end, a further experiment was conducted with the single-shot gallery setting with the WHOS feature, under the same human feedback protocol as described in Sec. 5.1.1 with the only difference that users were required to label visually

similar samples (weak negative) instead of dissimilar ones (strong negative). For model updates on weak negatives we adopted the same loss design of our preliminary model [76]. Table 6 shows that labelling weak negatives is much less effective than strong ones in re-id performance. For example, when weak negatives are labelled instead of strong ones, Rank-1 rates drop from 60.2%/53.7%/84.5% to 45.3%/43.6%/78.0% and Expected Ranks increase from 76.0/99.8/20.0 to 203.0/226.7/90.7 on CUHK03(Labelled/Detected) and Market-1501. Moreover, it is indicated by the users that weak negatives are much harder and time consuming to label. This is intuitive given that most top-ranked gallery images are visually similar which renders a user hard to select a specific one against the others (Fig. 4(c)).

5.2 Human-Out-of-the-Loop Re-id Evaluations

5.2.1 Experiment Settings

Finally, we assume that a limited budget for human verification on D_{p1}^i has been reached after time τ so that human feedback becomes unavailable. Re-id of any further independent population (e.g. D_{p2}^i) turns to a conventional human-out-of-the-loop (HOL) re-id problem, if one treats previously human labelled samples as training samples. The proposed RMEL model was then evaluated under this HOL re-id setting against both state-of-the-art supervised models and baseline ensemble models. This experiment was conducted with CNN feature on both CUHK03 (Labelled) and Market-1501 dataset. Additionally, to examine our proposed HVIL-RMEL framework in a more comparable context defined in the literature on HOL re-id, we also tested on the VIPeR [25] benchmark, with more details as follows.

Training/Testing protocol On CUHK03 and Market-1501 datasets, in each of the overall 10 trials, we employed the human verified true matches on D_{p1}^i to learn the weights for constructing a strong ensemble model using all the verified weak models $\{M_j\}_{j=1}^\tau$ collected from our previous experiments on human-in-the-loop re-id. The strong ensemble model was then deployed for testing on the separate partition D_{p2}^i with the size of 360 and 501 persons for CUHK03 and Market-1501 respectively. For performance evaluation, we adopted the standard single-shot test setting, i.e. randomly sampling 360 cross-camera person image pairs from CUHK03 and 501 pairs from Market-1501 on $\{D_{p2}^i\}_{i=1}^{10}$ to construct the test gallery and probe sets over ten trials. On VIPeR dataset, we followed the exact setting of the established protocol in existing literature: splitting the 632 identities into 50 – 50% partitions for training and testing sets. For obtaining weak re-id models, we simulated HVIL feedback update by simply giving only groundtrue matching pairs but no strong negatives (Eqn. (12)); therefore each weak model was obtained by a true-match, using the same information as training a conventional supervised model. On all three datasets the averaged CMC performance over all 10 trials was compared.

HOL Competitors On CUHK03 and Market-1501, six state-of-the-art supervised re-id models are compared⁵: kLFDA [88],

5. In this study, a challenging single-shot training/testing protocol (300/360 for CUHK03 and 300/501 for Market-1501) is adopted for HOL evaluation (Table 7). In contrast to the reported multi-shot setting [38,95] of 1260/100 for CUHK03 and 751/750 for Market-1501, this is a harder task.

6. Due to small training data, DGD (trained from scratch by design) runs into difficulty with converging therefore excluded in comparison, whilst Inception-V3 can avoid this problem by benefiting from model pre-training on ImageNet.

TABLE 7
Automatic person re-id (HOL) with CMC performances on CUHK03 and Market-1501. Gallery Size: 360 for CUHK03 and 501 for Market-1501⁵.

Dataset	CUHK03 ($N_g = 360$)				Market-1501 ($N_g = 501$)			
	1	5	10	20	1	5	10	20
kLFDA [88]	20.6	43.1	55.8	67.8	57.0	83.9	91.9	96.9
XQDA [39]	19.7	43.6	56.7	68.9	52.9	83.5	89.9	96.1
MLAPG [40]	15.8	35.8	45.6	57.7	52.2	78.6	87.7	94.1
NFST [91]	22.8	43.1	56.1	63.7	58.6	84.1	90.7	96.3
HER [75]	25.3	43.3	55.8	67.1	60.6	83.9	90.7	96.8
Inception-V3 [65]	18.3	37.8	50.0	63.1	56.2	81.7	88.5	93.6
HVIL - M_{avg}	19.7	39.2	55.3	70.3	57.3	85.5	93.0	96.5
HVIL - M_τ	20.3	43.3	56.4	66.1	59.3	86.8	93.6	96.5
HVIL - RMEL	21.9	46.7	59.2	71.4	62.6	87.0	92.3	96.3

TABLE 8
Automatic person re-id (HOL) with CMC performances on VIPeR.

Dataset	VIPeR ($N_g = 316$)			
	1	5	10	20
MLF [94]	29.1	52.3	66.0	79.9
kLFDA [88]	38.6	69.2	80.4	89.2
SCNCD [90]	33.7	62.7	74.8	85.0
XQDA [39]	40.0	68.1	80.5	91.1
MLAPG [40]	40.7	69.9	82.3	92.4
RKSL [77]	40.2	74.5	85.7	93.5
NFST [91]	42.3	71.5	82.9	92.1
LSSCDL [92]	42.7	-	84.3	91.9
HER [75]	45.1	74.6	85.1	93.3
RDC-Net [18]	40.5	60.8	70.4	84.4
JRL [11]	38.4	69.2	81.3	90.4
DGD [86]	38.6	-	-	-
Gated S-CNN [69]	37.8	66.9	77.4	-
S-LSTM [70]	42.4	68.7	79.4	-
MCP [12]	47.8	74.7	84.8	91.1
HVIL - M_{avg}	40.8	66.1	76.9	86.4
HVIL - M_τ	42.1	69.0	78.5	88.6
HVIL - RMEL	47.1	71.7	82.5	91.3

XQDA [39], MLAPG [40], NFST [91], HER [75], Inception-V3 [65]. The five metric learning methods were trained using 300 ground-truth labelled data from \mathcal{P}^i (300) and \mathcal{G}_s^i (1,000) of D_{p1}^i with the same CNN feature for both datasets. The Inception-V3 was first pre-trained on large ImageNet [35] data then fine-tuned on small re-id training data. The trained models were tested on the separate partition D_{p2}^i with same testing protocol as above. On VIPeR, as our training/testing protocol is standard, we compared fifteen recently published state-of-the-art including six deep models: RDC-Net [18], JRL [11], DGD [86], Gated S-CNN [69], S-LSTM [70], MCP [12], and nine shallow models: MLF [94], kLFDA [88], SCNCD [90], XQDA [39], MLAPG [40], RKSL [77], NFST [91], LSSCDL [92], HER [75]. Since all these existing methods utilised the same training/testing protocol, we directly compared ours with their reported results optimised by the original authors.

Metric Ensemble Baselines To investigate the metric ensemble effect by RMEL, two baseline methods are compared: (1) HVIL - M_τ : The incrementally optimised re-id model M_τ obtained by HVIL from the last probe image at time τ during the *human-in-the-loop* process. (2) HVIL - M_{avg} : A naive approach to ensemble weak models, that is, simply taking an average weighting of all weak models $\{M_j\}_{j=1}^\tau$ as the ensemble re-id model.

5.2.2 Evaluations on Person Re-Id Performance

Tables 7 and 8 report the results. For CUHK03, there is insufficient labelled data for all camera pairs during training, given only one pair of randomly selected single-shot images per identity. All the models generated poor re-id performances (Rank-1 rates < 30%), much less than state-of-the-art reported in the literature. For Market-1501, a similar problem exists although less pronounced. Note, the results in Table 7 are based on a single-shot test setting. This is a much harder problem than the multi-shot test setting [95] where on average 14.8 true matches exist in the gallery for each probe. Given the experimental results above, it is evident that: Due to (1) a larger unlabelled test gallery population than the labelled training set, (2) a lack of sufficient multi-shot training/testing data in many camera pairs, *human-in-the-loop* approach to re-id is not only desirable, but essential for re-id in real world applications.

Nevertheless, for HOL re-id, the HVIL-RMEL still achieves competitive performance among all the models with a Rank-1 of 21.9% (3.4% lower than HER (25.3%)) on CUHK03 and 62.6% (2.0% higher than HER (60.6%)) on Market-1501. Note that, the ensemble weighting for the RMEL model is learned by less true-match data (253 pairs for CUHK03 and 285 pairs for Market-1501), as compared to more ground-truth data (300 pairs for both benchmarks) used to train all other alternatives. This observation implies that by optimising re-id in a large gallery population with human in the loop, even a HOL re-id model (e.g. HVIL-RMEL) can benefit from stronger re-id generalisation to a new gallery search population. When HVIL-RMEL was evaluated under the standard training/testing setting on VIPeR, it yields 47.1% for Rank-1 rate, only 0.6% lower compared to the current best deep model MCP [12]. It is also evident that naively taking an average ensemble model (HVIL - M_{avg}) gives even poorer performance than the cumulatively learned single model (HVIL - M_T).

6 CONCLUSION

We formulated a novel approach to human-in-the-loop person re-id by introducing a Human Verification Incremental Learning (HVIL) model, designed to overcome two unrealistic assumptions adopted by existing fully automated re-id models that prevent them from being scalable to real world applications. In particular, the proposed HVIL model avoids the need for collecting offline pre-labelled training data and is scalable to re-id tasks in large gallery sizes in open world search scenarios. The advantage of HVIL over other human-in-the-loop models is its ability to learn cumulatively from human feedback on all probed images when available. We further developed a regularised metric ensemble learning (RMEL) method to explore HVIL for automated re-id tasks when human feedback is unavailable. Extensive comparisons on the CUHK03 [38], Market-1501 [95], and VIPeR [25] benchmarks show the potentials of the proposed HVIL-RMEL model for real-world re-id deployments. We also conducted extensively component evaluation and analysis for providing insights into the proposed HVIL model design.

ACKNOWLEDGEMENTS

This work was partly supported by the China Scholarship Council, Vision Semantics Ltd., the Royal Society Newton Advanced Fellowship Programme (NA150459), and Innovate UK Industrial Challenge Project on Developing and Commercialising Intelligent Video Analytics Solutions for Public Safety (98111-571149).

REFERENCES

- [1] London stations continue to dominate 'top of the stops' charts. [Online]. Available: <http://orr.gov.uk/news-and-media/press-releases/2015/london-stations-continue-to-dominate-top-of-the-stops-charts>
- [2] E. Ahmed, M. J. Jones, and T. K. Marks, "An improved deep learning architecture for person re-identification," in *CVPR*, 2015.
- [3] T. Ahonen, A. Hadid, and M. Pietikainen, "Face description with local binary patterns: Application to face recognition," *IEEE TPAMI*, vol. 28, no. 12, pp. 2037–2041, 2006.
- [4] Y. Amit and D. Geman, "Shape quantization and recognition with randomized trees," *Neural Computing*, vol. 9, no. 7, pp. 1545–1588, October 1997.
- [5] C. Arteta, V. Lempitsky, J. A. Noble, and A. Zisserman, "Interactive object counting," in *ECCV*, 2014.
- [6] L. Bottou, "Large-scale machine learning with stochastic gradient descent," in *COMPSTAT*, 2010.
- [7] S. Boyd and L. Vandenberghe, *Convex Optimization*. New York, NY, USA: Cambridge University Press, 2004.
- [8] S. Branson, C. Wah, F. Schroff, B. Babenko, P. Welinder, P. Perona, and S. Belongie, "Visual recognition with humans in the loop," in *ECCV*, 2010.
- [9] G. Chechik, V. Sharma, U. Shalit, and S. Bengio, "Large scale online learning of image similarity through ranking," *JMLR*, pp. 1109–1135, March 2010.
- [10] D. Chen, Z. Yuan, B. Chen, and N. Zheng, "Similarity learning with spatial constraints for person re-identification," in *CVPR*, 2016.
- [11] S.-Z. Chen, C.-C. Guo, and J.-H. Lai, "Deep ranking for person re-identification via joint representation learning," *IEEE TIP*, vol. 25, no. 5, pp. 2353–2367, 2016.
- [12] D. Cheng, Y. Gong, S. Zhou, J. Wang, and N. Zheng, "Person re-identification by multi-channel parts-based cnn with improved triplet loss function," in *CVPR*, 2016.
- [13] K. Crammer, O. Dekel, J. Keshet, S. Shalev-Shwartz, and Y. Singer, "Online passive-aggressive algorithms," *JMLR*, vol. 7, no. March, pp. 551–585, 2006.
- [14] Y. Cui, F. Zhou, Y. Lin, and S. Belongie, "Fine-grained categorization and dataset bootstrapping using deep metric learning with humans in the loop," in *CVPR*, 2016.
- [15] A. Das, R. Panda, and A. Roy-Chowdhury, "Active image pair selection for continuous person re-identification," in *ICIP*, 2015.
- [16] R. Datta, D. Joshi, J. Li, and J. Z. Wang, "Image retrieval: Ideas, influences, and trends of the new age," *CSUR*, pp. 5:1–5:60, April 2008.
- [17] J. V. Davis, B. Kulis, P. Jain, S. Sra, and I. S. Dhillon, "Information-theoretic metric learning," in *ICML*, 2007.
- [18] S. Ding, L. Lin, G. Wang, and H. Chao, "Deep feature learning with relative distance comparison for person re-identification," *Pattern Recognit.*, vol. 48, no. 10, pp. 2993–3003, 2015.
- [19] M. Farenzena, L. Bazzani, A. Perina, V. Murino, and M. Cristani, "Person re-identification by symmetry-driven accumulation of local features," in *CVPR*, 2010.
- [20] P. F. Felzenszwalb, R. B. Girshick, D. McAllester, and D. Ramanan, "Object detection with discriminatively trained part-based models," *IEEE TPAMI*, vol. 32, no. 9, pp. 1627–1645, 2010.
- [21] M. Geng, Y. Wang, T. Xiang, and Y. Tian, "Deep transfer learning for person re-identification," *arXiv e-prints*, 2016.
- [22] S. Gong, M. Cristani, C. L. Chen, and T. M. Hospedales, "The re-identification challenge," in *Person Re-Identification*. Springer, 2014.
- [23] S. Gong, M. Cristani, S. Yan, and C. C. Loy, *Person re-identification*. Springer, January 2014.
- [24] M. Grant and S. Boyd, "CVX: Matlab software for disciplined convex programming, version 2.1," <http://cvxr.com/cvx>, March 2014.
- [25] D. Gray, S. Brennan, and H. Tao, "Evaluating appearance models for recognition, reacquisition and tracking," in *IEEE International Workshop on Performance Evaluation for Tracking and Surveillance*, 2007.
- [26] M. Hirzer, C. Belezni, P. M. Roth, and H. Bischof, "Person re-identification by descriptive and discriminative classification," in *SCIA*, 2011.
- [27] T. M. Hospedales, S. Gong, and T. Xiang, "A unifying theory of active discovery and learning," in *ECCV*, 2012.
- [28] C. Huang, C. C. Loy, and X. Tang, "Local similarity-aware deep feature embedding," in *NIPS*, 2016.
- [29] P. Jain, B. Kulis, I. S. Dhillon, and K. Grauman, "Online metric learning and fast similarity search," in *NIPS*, 2009.
- [30] J. Kivinen and M. K. Warmuth, "Exponentiated gradient versus gradient descent for linear predictors," *Information and Computation*, pp. 1–63, 1997.

- [31] E. Kodirov, T. Xiang, Z. Fu, and S. Gong, "Unsupervised domain adaptation for zero-shot learning," in *ICCV*, 2015.
- [32] —, "Person re-identification by unsupervised l1 graph learning," in *ECCV*, 2016.
- [33] E. Kodirov, T. Xiang, and S. Gong, "Dictionary learning with iterative laplacian regularisation for unsupervised person re-identification," in *BMVC*, 2015.
- [34] M. Koestinger, M. Hirzer, P. Wohlhart, P. M. Roth, and H. Bischof, "Large scale metric learning from equivalence constraints," in *CVPR*, 2012.
- [35] A. Krizhevsky, I. Sutskever, and G. E. Hinton, "Imagenet classification with deep convolutional neural networks," in *Advances in neural information processing systems*, 2012, pp. 1097–1105.
- [36] S. Lad and D. Parikh, "Interactively guiding semi-supervised clustering via attribute-based explanations," in *ECCV*, 2014.
- [37] R. Layne, T. M. Hospedales, and S. Gong, "Domain transfer for person re-identification," in *ACM-MMW*, 2013.
- [38] W. Li, R. Zhao, T. Xiao, and X. Wang, "Deepreid: Deep filter pairing neural network for person re-identification," in *CVPR*, 2014.
- [39] S. Liao, Y. Hu, X. Zhu, and S. Z. Li, "Person re-identification by local maximal occurrence representation and metric learning," in *CVPR*, 2015.
- [40] S. Liao and S. Z. Li, "Efficient psd constrained asymmetric metric learning for person re-identification," in *ICCV*, 2015.
- [41] D. Lim and G. Lanckriet, "Efficient learning of mahalanobis metrics for ranking," in *ICML*, 2014.
- [42] W.-C. Lin, Z.-Y. Chen, S.-W. Ke, C.-F. Tsai, and W.-Y. Lin, "The effect of low-level image features on pseudo relevance feedback," *Neurocomputing*, 2015.
- [43] G. Lisanti, I. Masi, and A. Del Bimbo, "Matching people across camera views using kernel canonical correlation analysis," in *ICDSC*, 2014.
- [44] C. Liu, C. C. Loy, S. Gong, and G. Wang, "Pop: Person re-identification post-rank optimisation," in *ICCV*, 2013.
- [45] X. Liu, M. Song, D. Tao, X. Zhou, C. Chen, and J. Bu, "Semi-supervised coupled dictionary learning for person re-identification," in *CVPR*, 2014.
- [46] A. J. Ma, J. Li, P. C. Yuen, and P. Li, "Cross-domain person re-identification using domain adaptation ranking svms," *IEEE TIP*, vol. 24, no. 5, pp. 1599–1613, 2015.
- [47] A. J. Ma, P. C. Yuen, and J. Li, "Domain transfer support vector ranking for person re-identification without target camera label information," in *ICCV*, 2013.
- [48] N. Martinel, A. Das, C. Micheloni, and A. K. Roy-Chowdhury, "Temporal model adaptation for person re-identification," in *ECCV*, 2016.
- [49] T. Matsukawa, T. Okabe, E. Suzuki, and Y. Sato, "Hierarchical gaussian descriptor for person re-identification," in *CVPR*, 2016.
- [50] A. Mignon and F. Jurie, "Pcca: A new approach for distance learning from sparse pairwise constraints," in *CVPR*, 2012.
- [51] H. Oh Song, Y. Xiang, S. Jegelka, and S. Savarese, "Deep metric learning via lifted structured feature embedding," in *CVPR*, 2016.
- [52] S. Paisitkriangkrai, C. Shen, and A. van den Hengel, "Learning to rank in person re-identification with metric ensembles," in *CVPR*, 2015.
- [53] S. J. Pan and Q. Yang, "A survey on transfer learning," *IEEE TKDE*, vol. 22, no. 10, pp. 1345–1359, 2010.
- [54] D. Parkhurst, K. Law, and E. Niebur, "Modeling the role of salience in the allocation of overt visual attention," *Vision Research*, vol. 42, no. 1, pp. 107–123, 2002.
- [55] S. Pedagadi, J. Orwell, S. A. Velastin, and B. A. Boghossian, "Local fisher discriminant analysis for pedestrian re-identification," in *CVPR*, 2013.
- [56] L. Piras, G. Giacinto, and R. Paredes, "Passive-aggressive online learning for relevance feedback in content based image retrieval," in *ICPRAM*, 2013.
- [57] F. Rosenblatt, "The perceptron: A probabilistic model for information storage and organization in the brain," *Psychological Review*, 1958.
- [58] C. Rother, V. Kolmogorov, and A. Blake, "Grabcut: Interactive foreground extraction using iterated graph cuts," in *ACM Transactions on Graphics*, vol. 23, no. 3, 2004, pp. 309–314.
- [59] R. E. Schapire, "The strength of weak learnability," *Machine Learning*, vol. 5, no. 2, pp. 197–227, July 1990.
- [60] F. Schroff, D. Kalenichenko, and J. Philbin, "Facenet: A unified embedding for face recognition and clustering," in *CVPR*, 2015.
- [61] B. Settles, "Active learning literature survey," *University of Wisconsin, Madison*, vol. 52, no. 55-66, p. 11, 2010.
- [62] H. Shi, X. Zhu, S. Liao, Z. Lei, Y. Yang, and S. Z. Li, "Constrained deep metric learning for person re-identification," *arXiv e-prints*, 2015.
- [63] D. Singaraju, L. Grady, and R. Vidal, "Interactive image segmentation via minimization of quadratic energies on directed graphs," in *CVPR*, 2008.
- [64] C. Su, S. Zhang, J. Xing, W. Gao, and Q. Tian, "Deep attributes driven multi-camera person re-identification," in *ECCV*, 2016.
- [65] C. Szegedy, V. Vanhoucke, S. Ioffe, J. Shlens, and Z. Wojna, "Rethinking the inception architecture for computer vision," in *CVPR*, 2016.
- [66] K. Tsuda, G. Rätsch, and M. K. Warmuth, "Matrix exponentiated gradient updates for on-line learning and bregman projection," in *JMLR*, vol. 6, no. June, 2005, pp. 995–1018.
- [67] E. Ustinova, Y. Ganin, and V. Lempitsky, "Multiregion bilinear convolutional neural networks for person re-identification," *arXiv e-prints*, 2015.
- [68] N. Usunier, D. Buffoni, and P. Gallinari, "Ranking with ordered weighted pairwise classification," in *ICML*, 2009.
- [69] R. R. Varior, M. Haloi, and G. Wang, "Gated siamese convolutional neural network architecture for human re-identification," in *ECCV*, 2016.
- [70] R. R. Varior, B. Shuai, J. Lu, D. Xu, and G. Wang, "A siamese long short-term memory architecture for human re-identification," in *ECCV*, 2016.
- [71] C. Wah, S. Branson, P. Perona, and S. Belongie, "Multiclass recognition and part localization with humans in the loop," in *ICCV*, 2011.
- [72] J. Wan, P. Wu, S. C. Hoi, P. Zhao, X. Gao, D. Wang, Y. Zhang, and J. Li, "Online learning to rank for content-based image retrieval," 2015.
- [73] F. Wang, W. Zuo, L. Lin, D. Zhang, and L. Zhang, "Joint learning of single-image and cross-image representations for person re-identification," in *CVPR*, 2016.
- [74] H. Wang, S. Gong, and T. Xiang, "Unsupervised learning of generative topic saliency for person re-identification," in *BMVC*, 2014.
- [75] —, "Highly efficient regression for scalable person re-identification," in *BMVC*, 2016.
- [76] H. Wang, S. Gong, X. Zhu, and T. Xiang, "Human-in-the-loop person re-identification," in *ECCV*, 2016.
- [77] H. Wang, X. Zhu, T. Xiang, and S. Gong, "Towards unsupervised open-set person re-identification," in *ICIP*, 2016.
- [78] J. Wang, Y. Song, T. Leung, C. Rosenberg, J. Wang, J. Philbin, B. Chen, and Y. Wu, "Learning fine-grained image similarity with deep ranking," in *CVPR*, 2014.
- [79] T. Wang, S. Gong, X. Zhu, and S. Wang, "Person re-identification by discriminative selection in video ranking," *IEEE TPAMI*, vol. 38, no. 12, pp. 2501–2514, 2016.
- [80] —, "Person re-identification by video ranking," in *ECCV*, 2014.
- [81] X. Wang, W.-S. Zheng, X. Li, and J. Zhang, "Cross-scenario transfer person re-identification," *IEEE TCSVT*, vol. PP, no. 99, June 2015.
- [82] X. Wang and A. Gupta, "Unsupervised learning of visual representations using videos," in *ICCV*, 2015.
- [83] X. Wang, T. X. Han, and S. Yan, "An hog-lbp human detector with partial occlusion handling," in *ICCV*, 2009.
- [84] J. Weston, S. Bengio, and N. Usunier, "Large scale image annotation: Learning to rank with joint word-image embeddings," in *ECML*, 2010.
- [85] M. A. Woodbury, "Inverting modified matrices," *Memorandum Report*, vol. 42, p. 106, 1950.
- [86] T. Xiao, H. Li, W. Ouyang, and X. Wang, "Learning deep feature representations with domain guided dropout for person re-identification," in *CVPR*, 2016.
- [87] T. Xiao, S. Li, B. Wang, L. Lin, and X. Wang, "End-to-end deep learning for person search," *arXiv e-prints*, 2016.
- [88] F. Xiong, M. Gou, O. Camps, and M. Szaier, "Person re-identification using kernel-based metric learning methods," in *ECCV*, 2014.
- [89] B. Xu, J. Bu, C. Chen, D. Cai, X. He, W. Liu, and J. Luo, "Efficient manifold ranking for image retrieval," in *ASIGIR*, 2011.
- [90] Y. Yang, J. Yang, J. Yan, S. Liao, D. Yi, and S. Z. Li, "Salient color names for person re-identification," in *ECCV*, 2014.
- [91] L. Zhang, T. Xiang, and S. Gong, "Learning a discriminative null space for person re-identification," in *CVPR*, 2016.
- [92] Y. Zhang, B. Li, H. Lu, A. Irie, and X. Ruan, "Sample-specific svm learning for person re-identification," in *CVPR*, 2016.
- [93] R. Zhao, W. Ouyang, and X. Wang, "Unsupervised salience learning for person re-identification," in *CVPR*, 2013.
- [94] —, "Learning mid-level filters for person re-identification," in *CVPR*, 2014.
- [95] L. Zheng, L. Shen, L. Tian, S. Wang, J. Wang, and Q. Tian, "Scalable person re-identification: A benchmark," in *ICCV*, 2015.
- [96] W.-S. Zheng, S. Gong, and T. Xiang, "Associating groups of people," in *BMVC*, 2009.
- [97] —, "Re-identification by relative distance comparison," *IEEE TPAMI*, vol. 35, no. 3, pp. 653–668, March 2013.
- [98] X. S. Zhou and T. S. Huang, "Relevance feedback in image retrieval: A comprehensive review," *Multimedia Systems*, vol. 8, no. 6, pp. 536–544, 2003.